NCEP NOTES

Modeling of ^{137}Cs as a Tracer in a Regional Model for the Western Pacific, after the Fukushima–Daiichi Nuclear Power Plant Accident of March 2011

ZULEMA D. GARRAFFO AND HAE-CHEOL KIM

NOAA/NCEP/IMSG/Environmental Modeling Center, College Park, Maryland

AVICHAL MEHRA

NOAA/NCEP/Environmental Modeling Center, College Park, Maryland

TODD SPINDLER AND ILYA RIVIN

NOAA/NCEP/IMSG/Environmental Modeling Center, College Park, Maryland

HENDRIK L. TOLMAN

NOAA/NCEP/Environmental Modeling Center, College Park, Maryland

(Manuscript received 27 August 2013, in final form 30 June 2014)

ABSTRACT

In this study, results are presented from the first operational ocean tracer dispersion model operated by the National Oceanic and Atmospheric Administration/National Weather Service/National Centers for Environmental Prediction (NOAA/NWS/NCEP). This study addresses the dispersion of radionuclide contaminants after the Fukushima–Daiichi nuclear accident that was triggered by the 11 March 2011 earthquake and tsunami. The tracer capabilities of the Hybrid Coordinate Ocean Model (HYCOM) were used in a regional domain for the northwestern Pacific, with nesting lateral boundary conditions using daily nowcast–forecast fields from the global operational Real-Time Ocean Forecast System (RTOFS-Global), a $1/12°$ HYCOM global forecast from NCEP, based on data-assimilative $1/12°$ HYCOM Global Ocean Forecast System (GOFS) analyses from the Naval Research Laboratory/Naval Oceanographic Office (NRL/NAVOCEANO). This regional model, RTOFS Episodic Tracers for a region of the North West Pacific (RTOFS-ET_WPA), was in operation until the beginning of 2014, when the simulated ^{137}Cs concentration was very close to the background level in the Pacific before the accident, which was about 2 Becquerel m^{-3} [Bq; 1 Becquerel = 1 (nuclear decay) s^{-1}].

1. Introduction

The Tōhoku earthquake that occurred on 11 March 2011 was the most powerful earthquake known to have hit Japan (moment magnitude M_w of 9.03). The tsunami triggered by this huge earthquake damaged the Fukushima–Daiichi Nuclear Power Plant (FNPP) complex (37°25′N, 141°2′E); after backup power was lost, three of the reactor cores in the power plant partially melted. While efforts to cool down the reactors were made, the melted fuel caused explosions, resulting in the emission of significant amounts of radioactive materials into the atmosphere, transported and dispersed by winds, and partially deposited into the ocean (Chino et al. 2011; Stohl et al. 2012; Morino et al. 2011).

Of the radionuclides of concern for humans and the food chain (^{131}I, ^{134}Cs, and ^{137}Cs), ^{131}I does not have a long-term presence since it rapidly decays with a half-life of 8.02 days. The cesium components are important, due to their half-life of 2.06 yr for ^{134}Cs and 30.17 yr for ^{137}Cs. Deposition of ^{134}Cs and ^{137}Cs into the Pacific Ocean, and consequently their dispersion/transport, occurred in an initial activity ratio very close to 1:1

Corresponding author address: Zulema D. Garraffo, IMSG, NOAA/NCEP/Environmental Modeling Center, 5830 University Research Ct., College Park, MD 20740.
E-mail: zulema.garraffo@noaa.gov

DOI: 10.1175/WAF-D-13-00101.1

during the Fukushima accident (Buesseler et al. 2011, 2012). This unit value of the ^{134}Cs to ^{137}Cs ratio at the source further allows identification of radionuclides as having Fukushima origin or not.

A number of studies have been conducted recently to estimate the total amount of radionuclides dispersed in the atmosphere and later deposited over both land and ocean in the vicinity of the disaster. By coupling environmental monitoring data with atmospheric dispersion simulations, Chino et al. (2011) estimated the rates and total amounts of radionuclides released into the atmosphere from 12 March 2011 to 4 June 2011, totaling 13 peta-Becquerel [where 1 Becquerel (Bq) = 1 (nuclear decay) s^{-1} and 1 peta-Becquerel (PBq) = 10^{15} Bq] for ^{137}Cs. This work was the basis for the Nuclear Safety Commission of Japan (NSC) disclosure for the total radionuclide discharge into the atmosphere (12 PBq of ^{137}Cs reported on 12 April 2011). Morino et al. (2011) simulated deposition rates from atmospheric radioactive materials (^{131}I and ^{137}Cs) with a three-dimensional atmospheric chemical transport model including dry and wet deposition, in a region of about 8° × 8° centered at the Fukushima location. Their estimate of ^{137}Cs emission for only the month of March 2011 was 9.9 PBq, of which 4.4 PBq was deposited over both land and ocean in the modeled region. Stohl et al. (2012) presented an estimation of radionuclide emissions, obtained from an inverse method with atmospheric dispersion models and measurements over Japan, North America, and other regions. Their ^{137}Cs inversion results gave a total emission of 36.6 PBq (20.1–53.1 PBq). This wide range for emission estimations (9.9–36.6 PBq) can be attributed to limited data availability and differences in atmospheric modeling frameworks (resolution, parameterizations, etc.) and are an indication of the uncertainty in the atmospheric source. We discuss atmospheric sources in section 3b(4).

Observations of radionuclide concentrations in surface and subsurface waters are crucial for assessing the local contamination near the accident site, as well as radionuclide transport by the atmosphere and ocean. Concentrations of ^{137}Cs in the direct vicinity of the FNPP after the accident were observed and made publicly available by the Tokyo Electric Power Company (TEPCO) and by the Ministry of Education, Culture, Sports, Science and Technology–Japan (MEXT); their results were discussed by Buesseler et al. (2011). According to Buesseler et al. (2011), the TEPCO data at two discharge channels and two coastal locations show ^{137}Cs peak concentrations in April 2011 at the channels ($\approx 0.7 \times 10^8$ Bq m^{-3} in the northern channel). These concentrations then decrease, reaching values of about 10^5 Bq m^{-3} in the following month. High concentrations extended to the MEXT locations 30 km offshore, where they reached values of 10^5 Bq m^{-3} by mid-April. Buesseler et al. (2012) measured radionuclide concentrations during June 2011 in surface and subsurface waters and in mesopelagic fish and plankton in the region 30–600 km off Japan at 34°–38°N, and sampled the circulation with drifters. The maximum concentrations were found in a semipermanent nearshore eddy (^{137}Cs concentrations above 3000 Bq m^{-3}). They found that the Kuroshio formed a southern boundary for the transport of the Fukushima-derived radionuclides, with water samples to the north of the current containing ^{134}Cs, but those within the current or south of it showing no significant amount of ^{134}Cs. Observations were reported by Honda et al. (2012) during April–May 2011 for surface seawater ^{137}Cs concentrations, in sections with end points at a distance 1800 km northeast and 900 km southeast of Fukushima, and passing 200 and 400 km east of Fukushima. Observed values ranged between 4 and 284 Bq m^{-3}. Observations from commercial and cargo ships and research vessels during April–May 2011 and March 2011–March 2012 were presented by Aoyama et al. (2012, 2013), which include Honda et al.'s stations. In April 2011, surface concentrations of ^{137}Cs larger than 1000 Bq m^{-3} were found several hundred kilometers east of Fukushima. Values larger than 100 Bq m^{-3} were also found in May 2011 near 43°N, 180°, more than 3000 km from the source. These measurements indicate that the main radioactive plume, formed by both atmospheric deposition and direct discharge, traveled eastward away from the source, advected and diffused by the Kuroshio and extension and related mesoscale eddies, with the Kuroshio playing a role of a barrier and retaining most of the surface tracer north of the current.

Several modeling studies have addressed the coastal and large-scale dispersion of contaminants. Regarding nearshore models, Masumoto et al. (2012) presented an intercomparison of ocean simulations for the direct deposition of contaminants near the Fukushima nuclear complex [including models in Kawamura et al. (2011), Tsumune et al. (2012), and Estournel et al. (2012)], in which the total directly discharged activity of ^{137}Cs was estimated to be 2–15 PBq based on various sources. These simulations showed an initial southward transport due to a weak coastal current, followed by transport and dispersion by mesoscale eddies and the eastward-flowing Kuroshio. Among the studies for dispersion including the ocean interior, Dietze and Kriest (2012) simulated the evolution of the coastal discharge of ^{137}Cs using a global model with enhanced resolution near Fukushima for times up to 1 yr. They estimated a residence time of 43 (±26) days of ^{137}Cs on the shelf; forecasted an eastward progression of the ^{137}Cs patch, with enhanced surface activity offshore a few months after the release; and predicted the presence of tracer in the Kuroshio–Oyashio region (a site of North Pacific Intermediate Water formation) 1 yr after the release. For time scales of a few months, Rypina et al. (2013) presented numerical simulations of radionuclides aiming at interpreting the observations of Buesseler et al. (2012), through simulated Lagrangian particles. They used both two-dimensional surface velocities (geostrophic velocities from altimetry plus Ekman velocities) and three-dimensional velocities from a high-resolution (3 km) Navy Coastal Ocean Model (NCOM) simulation with data assimilation covering a region 15° latitude × 20° longitude off the coast of Fukushima. They found better agreement with the observations for a direct ocean discharge of about 16 PBq. The long-term and basin- to global-scale evolution of the Fukushima tracer was studied by Behrens et al. (2012) and Rossi et al. (2013). Behrens et al. (2012) presented long-term (10 yr) basin- to global-scale simulations of ^{137}Cs after the Fukushima nuclear accident forced with 10 yr atmospheric reanalysis products (ending in 2007). The tracer spread through transport by large-scale currents and eddies, and was vertically mixed by turbulence mostly in winter. The tracer dispersed in a large region in the central Pacific 2½ years after the initial release, covering approximately 25°–45°N, 160°E–140°W; penetrating to depths of more than 400 m; and leaving a 20° × 15° region off the coast of Japan free of tracer. Rossi et al. (2013) indicated that ^{137}Cs is expected to reach the U.S. West Coast by early 2014 with concentrations $>10\,\mathrm{Bq\,m^{-3}}$. The numerical studies predicted a general eastward evolution, location north of Kuroshio at the initial stages, with later penetration south of the current, and dilution of the tracer, from months to decades in advance.

Many of these modeling studies focus on the evolution of ^{137}Cs from direct coastal discharge as it disperses into the ocean. In the present work we follow the evolution of ^{137}Cs originating from the Fukushima–Daiichi nuclear power plant accident, after it was injected into the ocean both through atmospheric deposition and coastal discharge, and for a 2–3 yr time frame. Here, we use an operational framework. Results of the simulation are produced in real time after April 2011, and have been publicly available in real time since a few months after the accident. The first objective of the simulations is to obtain results that can be used for quick guidance on environmental contamination that could be provided as actionable information to managers and decision makers. In addition, the tracer simulations at National Weather Service/National Centers for Environmental Prediction (NWS/NCEP) serve as a practical example for future operational implementation of ecobiological ocean forecasts with realistic currents.

This paper is organized as follows. In section 2, the regional ocean model and the atmospheric and direct discharge sources are described. In section 3, the results of the simulation are presented and discussed. In section 4, we summarize our results and present our conclusions.

2. ^{137}Cs simulations

This study is part of a bigger effort started immediately after the accident with preliminary estimations of contaminant transport made via synthetic particles advected offline using velocity fields of the global operational Real-Time Ocean Forecast System (RTOFS-Global; Tolman et al. 2013; see appendix A). These preliminary estimations allowed a quick assessment of regions where radionuclides were transported, and produced a rough estimation of radionuclide concentrations that was provided to the U.S. government in near–real time through an Interagency Working Group (Tolman et al. 2013).

Our present modeling study that traces both atmospheric and oceanic discharge consists of a nested regional ocean model with one tracer [RTOFS Episodic Tracers for a region of the North West Pacific (RTOFS-ET_WPA)] and no data assimilation. It makes use of different components, including a global ocean model, an atmospheric dispersion model, and a coastal ocean model. The simulation and components involved are listed in Table 1, and are described in detail in the next sections. RTOFS-ET_WPA is initialized for the day of the accident from a global hindcast (RTOFS-Global) that does not contain tracers. The tracer deposited from the atmosphere is input at the ocean surface as per the estimates by an atmospheric dispersion model (Draxler et al. 2013) produced by the National Oceanic and Atmospheric Administration (NOAA) Air Resources Laboratory (ARL) for the days following the accident (through 17 April 2011). The coastal discharge is added to the existing tracer on 26 April 2011 from a three-dimensional tracer distribution simulated by a high-resolution coastal model configured by NOAA/National Ocean Service (NOS). After that, the tracer evolved in RTOFS-ET_WPA with no extra sources and no radioactive decay.

a. Regional ocean model for the western Pacific

RTOFS-ET_WPA uses HYCOM in a configuration with 1/12° resolution in the horizontal, nested in the 1/12° RTOFS-Global model with no tracer running operationally at NOAA/NCEP (http://polar.ncep.noaa.gov/global; http://www.ncep.noaa.gov/newsletter/january2012; description in appendix B and Table 1). RTOFS-ET_WPA makes use of the HYCOM tracer capabilities, which solve the prognostic tracer equations including turbulence parameterization at each time step. The model

TABLE 1. Model components. The RTOFS-ET_WPA simulated dates, and the dates for the inputs, are listed.

Name	Configuration	Domain	Usage
RTOFS-ET_WPA	HYCOM 1/12°, one tracer, no data assimilation, atmospheric forcing: NCEP GDAS (past) and NCEP GFS (future)	Northwestern Pacific Ocean (Fig. 1)	Tracer simulations during 11 Mar 2011–Dec 2013
Input			
RTOFS-Global (appendix B)	HYCOM 1/12°, no tracer, daily analysis (NAVOCEANO), atmospheric forcing: NCEP GDAS (past) and NCEP GFS (future)	Global	Initial conditions on 11 Mar 2011 and lateral boundary conditions for 2011–13
HYSPLIT-NSC	HYSPLIT atmospheric dispersion model, ^{137}Cs from Chino et al. (2011), 0.25° NOAA GDAS winds	Global	Deposition of tracer applied during 11 Mar–10 Apr 2011
Coastal model (NOS-ROMS)	ROMS 1 km (NOAA/NOS)	Coastal (Figs. 1, 3)	Direct discharge applied on 26 Apr 2011
Atmospheric forcing			
NCEP GDAS	Atmospheric spectral model (appendix B)	—	For hindcasts with data assimilation
NCEP GFS	Atmospheric spectral model (appendix B)	—	For forecasts initialized from GDAS

includes one tracer, with no radioactive decay, for ^{137}Cs, since its half-life (unlike ^{134}Cs and ^{131}I) is much longer than the 2–3-yr simulation time. The RTOFS-ET_WPA HYCOM source (release version 2.2.36) is modified to include atmospheric deposition of tracers in the following manner. Starting with a zero ^{137}Cs concentration at the beginning of the simulation, the atmospheric deposition tracer corresponding to each model time step is added as a concentration distributed over the model top layer with a thickness of 1 m (see section 2b and Table 1 for details on the atmospheric tracer source). The tracer is rapidly mixed throughout the mixed layer via the turbulent parameterizations in the *K*-profile parameterization (KPP) mixed layer of RTOFS-ET_WPA, in which the tracer is treated like salinity for turbulent vertical mixing. The mixed layer depth (MLD) is defined as the depth at which the density difference with respect to the surface is equivalent to a 0.3°C temperature change (with no change of salinity). The model covers the western North Pacific region inside 15.3°–58°N and 133.7°E–150°W (Fig. 1). The horizontal grid, a subset of the global model, is a Mercator grid except north of 47°N. The vertical structure is solved in 32 vertical layers, of which the top 7 layers are generally in z coordinates and cover the upper 30 m, with 1- and 2-m thicknesses for the top two layers. The model is initialized with the nowcast state of RTOFS-Global for 11 March 2011, and is run with no updates to the global data-assimilated solutions in the interior of the domain. The lateral boundary conditions are from one-way nesting, with the external solution being daily nowcast states of the RTOFS-Global simulation, which include data assimilation in their daily initialization (appendix B). The one-way nesting method applies the method of characteristics for normal barotropic velocity and pressure, while parallel barotropic velocities are imposed. Normal baroclinic velocities and total mass fluxes are imposed while tangential velocities are nudged at the boundary. Because data assimilation is present only in the lateral boundary conditions, which are not enough to constrain the ocean interior, except for the first few days from initialization, the model ocean interior is not expected to reproduce the oceanic eddy field and the Kuroshio frontal location of the real ocean.

Keeping the regional model with no updates to the interior of the data-assimilated global model is a simple way to have the tracer follow the ocean dynamics at the model resolution. This procedure was adopted because at the time of the accident, a tracer correction capability was not available that worked well in conjunction with updates of the physical variables to those of RTOFS-Global and updates on the open model boundaries. Future developments are expected to include corrections to tracers concordant with data-assimilative corrections in the thermodynamic variables, geopotential, and velocities.

In operations, each day RTOFS-ET_WPA is advanced for 1 day (to the present), and in addition one forecast day is produced. The forcing employed is the

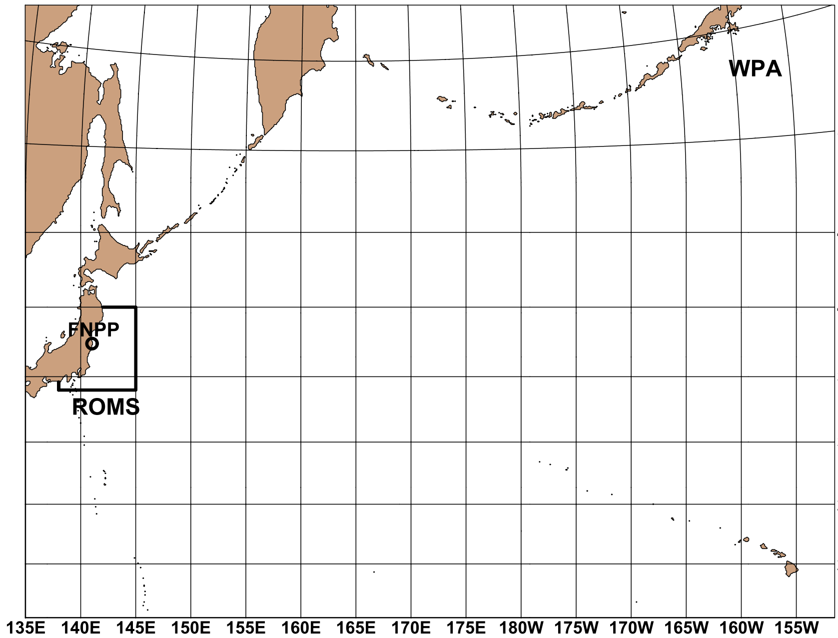

FIG. 1. Total domain of RTOFS-ET_WPA (indicated as WPA) represented with its points equally spaced, and the domain of NOS-ROMS (indicated as ROMS) shown with thick lines. FNPP is indicated.

same NCEP forcing as for RTOFS-Global, based on a global spectral atmospheric model, which includes satellite and atmospheric data assimilation for times in the past (Yang et al. 2006; see Table 1 and appendix B; Saha et al. 2010).

b. *Source for atmospheric deposition of ^{137}Cs*

NOAA/ARL produced several estimations of the atmospheric deposition of radionuclides from the FNPP with their atmospheric dispersion model, the Hybrid Single Particle Lagrangian Integrated Trajectory Model (HYSPLIT; Draxler and Hess 1998; Draxler et al. 2013, 2014). A version close to Draxler et al. (2013), which included ^{137}Cs sources from the Japan Nuclear Safety Commission (HYSPLIT-NSC), is used for this study. The HYSPLIT-NSC source for ^{137}Cs is based on Chino et al. (2011), who included verification with environmental monitoring data (see Table 1 for HYSPLIT-NSC). The total deposition of ^{137}Cs over land and ocean in HYSPLIT-NSC was approximately 10 PBq. This atmospheric dispersion model tested successfully (Draxler et al. 2013) in evaluations of ^{137}Cs depositions over land obtained from different global meteorological analyses using a common emission source.

According to this source for ^{137}Cs, the time-integrated tracer concentration (Fig. 2a) reached a maximum in a region extending about 100 km around the nuclear plant. The maximum value was $3.8 \times 10^6\,\mathrm{Bq\,m^{-2}}$. Values greater than $10^4\,\mathrm{Bq\,m^{-2}}$ extended several hundred kilometers from the plant, and some tracer (with deposition concentrations up to $1000\,\mathrm{Bq\,m^{-2}}$) was deposited in the Bering Sea. The deposition occurred during the period 13 March–17 April 2011 (Fig. 2b). In the first 100 km from the plant, 46% of the total tracer was deposited, and 25%, 11%, 12%, and 5% were deposited at distances 100–500, 500–1000, 1000–2000, and >3000 km from the plant, respectively. The total ^{137}Cs amount deposited through the atmosphere over the ocean was 5.4 PBq (Fig. 2b). Of the total deposition, 83% occurred north of the Kuroshio front, defined as collocated with the mean for the days of deposition of the 0.3-m sea surface height (SSH) contour.

c. *Addition of coastal discharge from a coastal ocean simulation*

We included the direct discharge of contaminated water into the ocean by adding the tracer distribution from a very high-resolution ocean model with the Regional Ocean Modeling System (ROMS) from NOAA/NOS, which is one of the models participating in the comparison for coastal discharge by Masumoto et al. (2012). This model covered the region 34°–40°N, 138°–145°E, with 1-km horizontal resolution and 50 sigma vertical layers (Figs. 1 and 3), and was nested in the data-assimilating

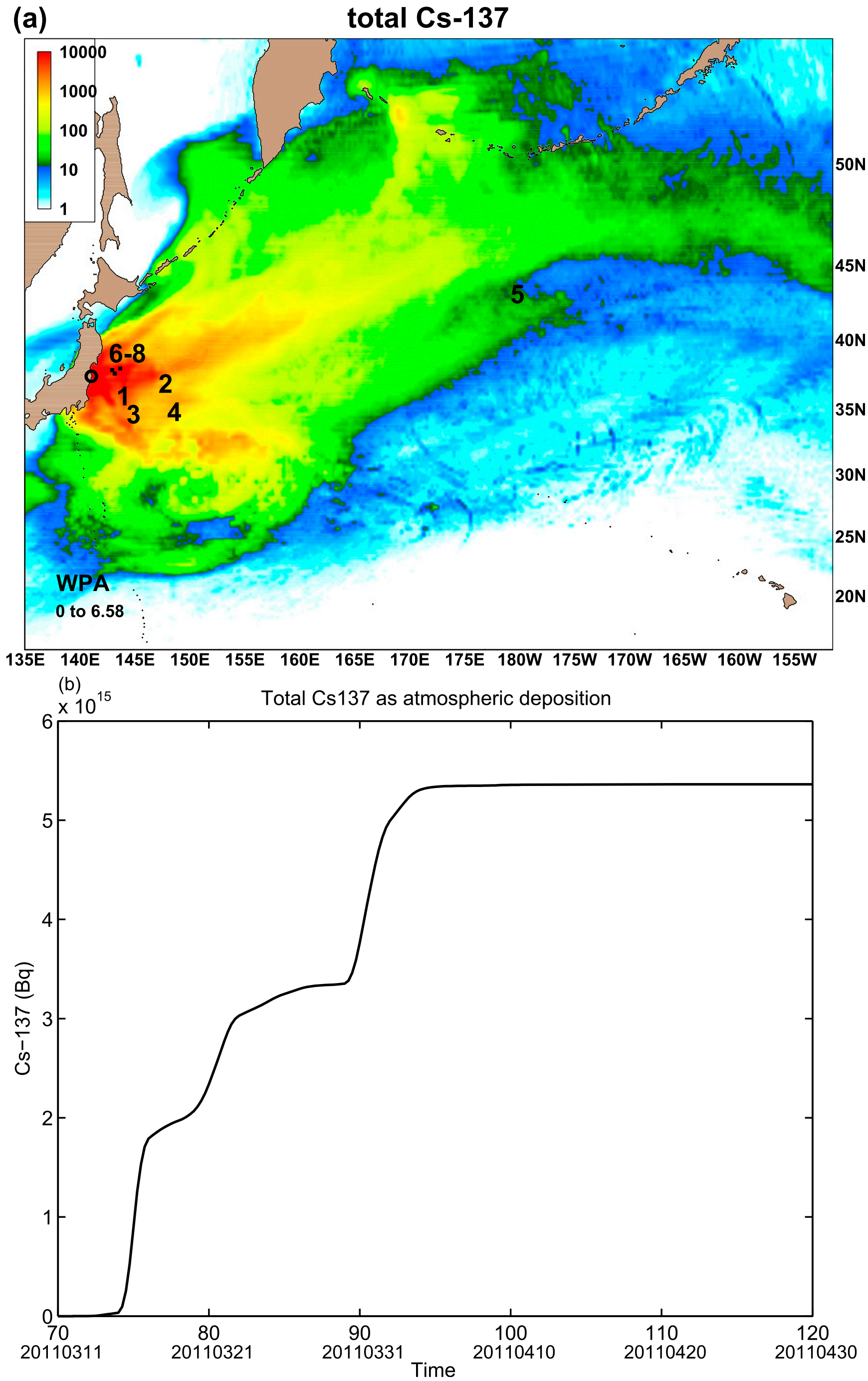

FIG. 2. Atmospheric deposition of ^{137}Cs according to HYSPLIT-NSC. (a) Horizontal distribution of the total deposition (Bq m^{-2}), with a max value of 3.8×10^6 Bq m^{-2} (or 6.58 in $\log_{10}$ scale), in the RTOFS-ET_WPA domain. The locations of FNPP (circle) and Table 4 observations 1–8 (1–5 are numbers; 6–8 are dots at the observed locations and numbers) are indicated. (b) Time dependence of the distribution of the accumulated deposition (accumulated from the initial time vs time in Julian days since 1 Jan 2011, with dates indicated) over the whole domain (PBq) as obtained from the ocean simulation.

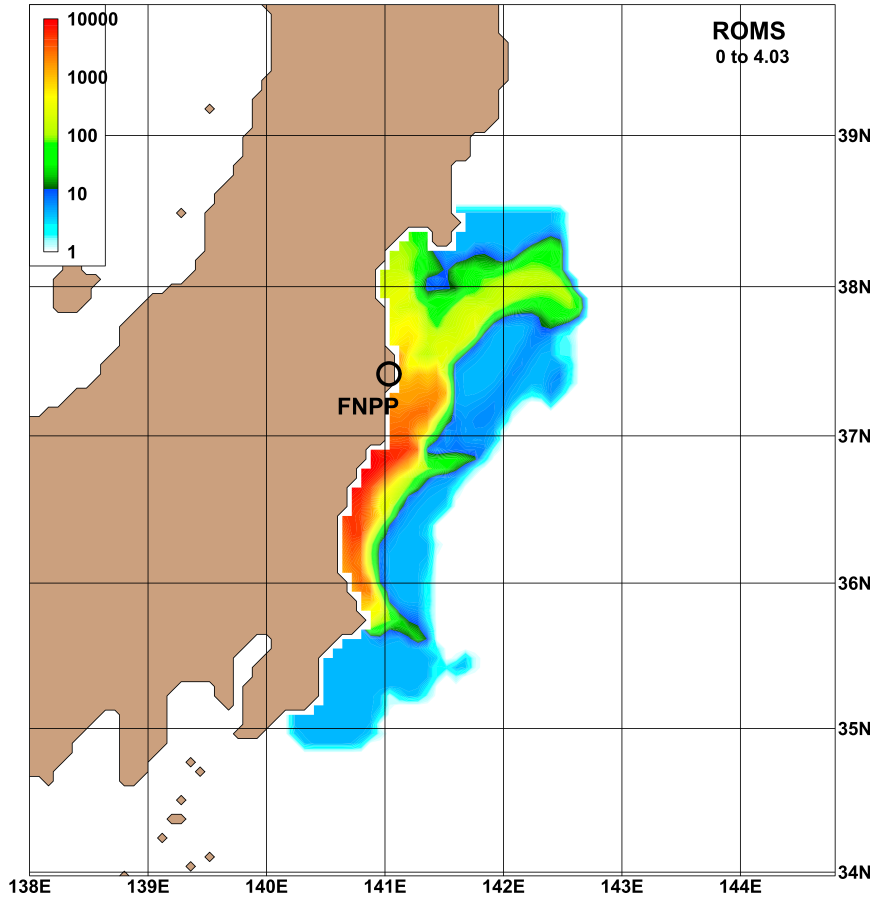

FIG. 3. Surface concentration of ^{137}Cs due to coastal discharge (Bq m^{-3}), as obtained from NOS-ROMS for 26 Apr 2011, renormalized and interpolated onto the RTOFS-ET_WPA grid, shown in the total domain of NOS-ROMS. The location of FNPP (circle), min concentration (0), and $\log_{10}$ of the max concentration are indicated.

NCOM (Barron et al. 2004). All simulations in Masumoto et al. (2012) show the tracer initially following a southward coastal surface current. At the end of April 2011, the NOS-ROMS surface tracer concentration is considerably lower than that observed and than those from other simulations with a similar total source [see Masumoto et al. (2012), NOAA simulation]. This may indicate an unrealistically high vertical diffusion for NOS-ROMS. The coastal source in NOS-ROMS was a version of the estimate by Kawamura et al. (2011), at the Japan Atomic Energy Agency (JAEA), which resulted in 4.5 PBq for coastal discharge [this was 4 PBq in Kawamura et al. (2011)]. In this coastal simulation, the total tracer begins to decrease in May 2011 due to advection of tracer out of the modeled region. Therefore, we interpolated the NOS-ROMS 26 April 2011 tracer distribution to the horizontal and vertical model grid of RTOFS-ET_WPA for that day. To eliminate background noise, only tracer values greater than 3 Bq m^{-3} were kept, and in addition the tracer was limited to the region 34.9°–38.5°N (surface tracer in Fig. 3). The tracer inventory was then renormalized to the NOS-ROMS total tracer content of 4.5 PBq. The tracers from atmospheric deposition and coastal discharge were 5.4 and 4.5 PBq, respectively, which totaled 10 PBq.

After the inclusion of the NOS-ROMS direct coastal discharge (Fig. 4), the combined tracer evolved in the RTOFS-ET_WPA model with no additional tracer sources. Our simulation with atmospheric deposition and coastal discharge covered the period from 26 April 2011 through the beginning of 2014. In the last few months of the simulation, the ^{137}Cs maximum concentrations were less than 5 Bq m^{-3}, close to the background concentration of 1–2 Bq m^{-3} prevalent in the Pacific prior to the Fukushima accident, due to natural processes, nuclear tests performed during the 1960s, and a very small contribution from the Chernobyl nuclear

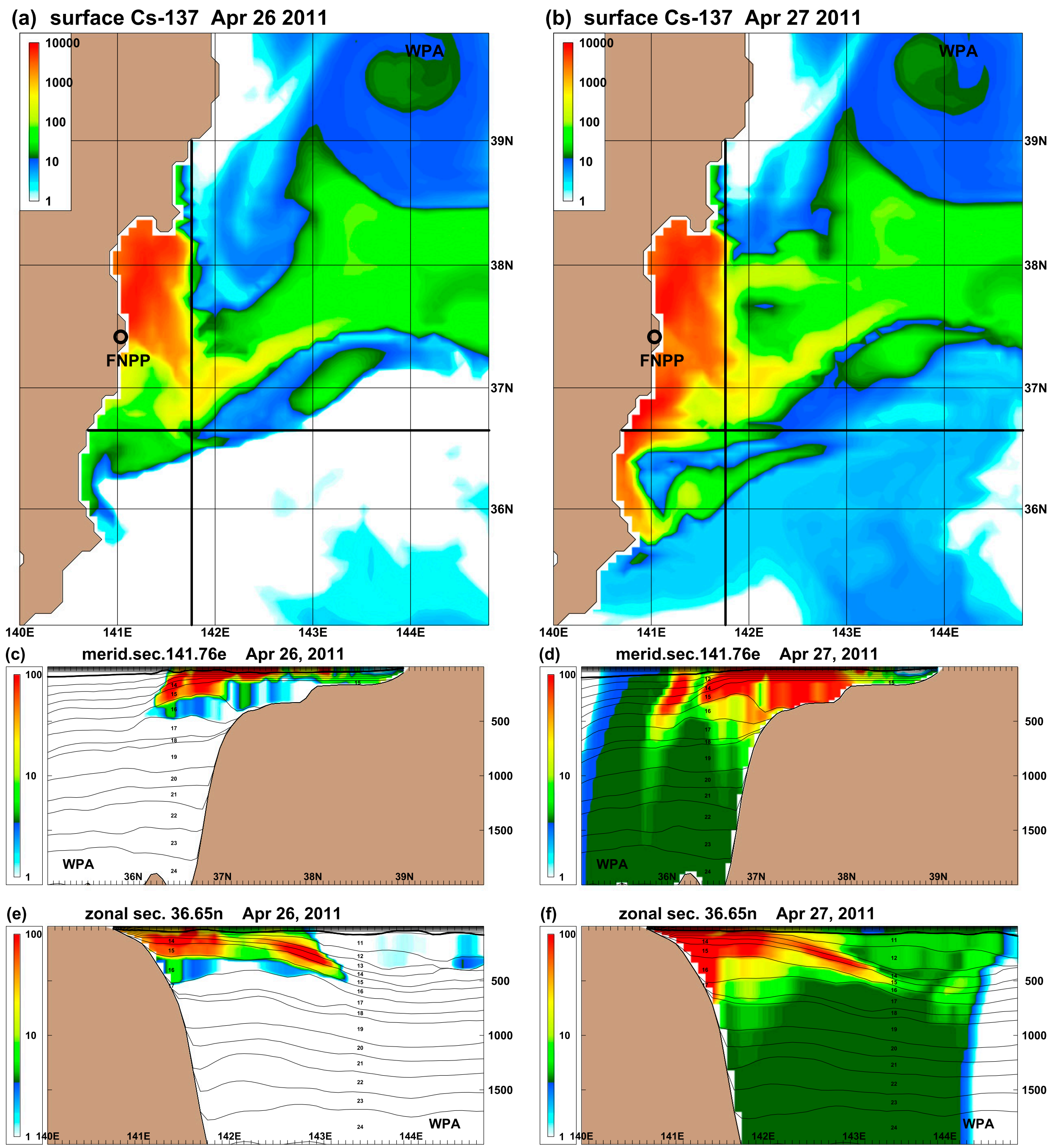

FIG. 4. Concentration of ^{137}Cs (Bq m^{-3}). The surface concentration from RTOFS-ET_WPA in the region close to Fukushima is equal to the total domain of NOS-ROMS: (a) 26 Apr 2011, model forced with atmospheric deposition only, after the end of the deposition period; (b) 27 Apr 2011, immediately after adding the direct ocean discharge from the coastal model; (c),(d) as in (a),(b), but for the meridional section at 141.76°E; and (e),(f) as in (a),(b), but for the zonal section at 36.65°N. In (a),(b), the locations of the FNPP (circle) and the zonal/meridional sections (thick lines) are indicated.

accident of 1986 (Aoyama et al. 2012, 2013). In addition, we did not account for the tracer leaving the RTOFS-ET_WPA model boundaries, for which reason we consider the simulation meaningful only through the first half of 2013.

It should be noticed that tracer released from coastal locations after April 2011 is not included in our simulation, while discharge, though in smaller than the initial amounts, was reported through 2011 and 2012 (Kanda 2013), and is probably continuing.

3. Results and discussion

a. Simulated ocean circulation in the northwestern Pacific

The circulation (Fig. 5) in our model, which was initialized with a data-assimilated solution in March 2011 and was evolved forward with lateral boundary conditions from RTOFS-Global nowcasts with no extra interior reinitialization or data assimilation, begins with and develops many of the same features seen in the observations. The annual mean circulation in the Kuroshio and Kuroshio Extension (KE) shown in Fig. 5a compared well with the drifter-derived velocities of Niiler et al. (2003) for the 1990s (their Figs. 2 and 5; not shown). Two meanders on the KE formed east of Japan at 144° and 150°E (indicated as m1 and m2 in Fig. 5a) as reported by past observations (Kawai 1972; Mizuno and White 1983; Niiler et al. 2003), and a third meander (m3) with a northward deflection at 158°E was formed slightly westward than that reported by Niiler et al. (2003). East of this last meander, the northern branch is apparent, located east of 160°E near 36°N. In comparison with Niiler et al. (2003), the model anticyclonic recirculation region south of the Kuroshio and west of 140°E (a1) showed good agreement, while the anticyclonic recirculation south of the first two meanders of the KE (a2) showed a somewhat different extent, with a cyclonic eddy (c1) present south of the first meander (Yasuda et al. 1996). Part of this difference can be due to the different time periods used for averaging in the model and observations. Downstream of the Tsugaru Strait and located between the islands of Honsu and Hokkaido, the Tsugaru coastal current, a branch that joins the subpolar front and contributes to the Subarctic Current, and an anticyclonic eddy (a3) north of the second KE meander are in agreement with Niiler et al. (2003). The southward Oyashio current flows east of the island of Hokkaido. The model circulation is also in agreement with the currents and eddies of the circulation schemes reported in Yasuda et al. (1996) and Yasuda (2003). Overall, the 15-m-depth circulation pattern from the model agrees very well with Niiler et al. (2003) for the Kuroshio and KE, with the northern branch at 36°N, the southern branch at 32°N, and the subpolar front at 40°N.

The surface instantaneous and annual mean velocity in the western region of the Kuroshio and KE are compared (Fig. 5) with surface geostrophic velocities derived from satellite altimetry data provided by Archiving, Validation, and Interpretation of Satellite Oceanographic data (AVISO; http://www.aviso.oceanobs.com). For a qualitative assessment in a region of strong currents, we consider this comparison valid even though the Ekman component is missing in the observations. The contribution of the Ekman component to the climatological 15-m total velocity was visually unnoticeable (not shown), based on the total and geostrophic velocities from the NOAA/Atlantic Oceanographic and Meteorological Laboratory (AOML) drifter climatology by Lumpkin and Garraffo (2005). For 27 April 2011 (Fig. 5b), the surface velocity in the Kuroshio front ranges between 1 and 2.5 $\mathrm{m\,s^{-1}}$, while the annual averaged velocity (May 2011–April 2012; Fig. 5d) shows values on the front between 0.6 and 1.2 $\mathrm{m\,s^{-1}}$ (the observed maximum values are about 1.3 $\mathrm{m\,s^{-1}}$ in Figs. 5c,e). The modeled and altimeter-derived velocities compare closely for 27 April 2011 (Figs. 5b,c), with the location of the two semipermanent meanders discussed above (m1 and m2) in close agreement, except that the second model meander and the eddy north of it (a4) are located 1°–2° toward the west of the observed features. The eddy at 39°N, 144°E (a5) is also reproduced by the model. South of the KE, the model shows cyclonic and anticyclonic eddies. The cyclonic eddy south of the second southward meander of the KE (c2, 31.5°N, 153°E) is in good agreement with the observations, while the anticyclonic eddies immediately south of the KE at 145° and 151°E (a6 and a7) are more developed and slightly displaced in the model compared with the observations. The good representation in the model of the main observed mesoscale features indicates a lasting impact of the realistic hindcast initialization through April 2011, 1.5 months after initialization. Even after omitting very narrow currents or filaments unresolved in the 1/3° gridded observations, away from the main current, the model generally shows an overabundance of high-velocity features relative to the observed geostrophic velocity field.

The annual mean model velocity shows that the two meanders of the KE (m1 and m2) are in agreement with the observed geostrophic velocity (Figs. 5d,e), but the modeled velocities east of 152°E are weaker than those observed. The narrower model Kuroshio and KE, with respect to the observations, indicate weaker modeled than observed current path fluctuations. The difference in the model and observed magnitudes, not present for April 2011, indicates that the circulation weakened in the KE during the year of the average (Fig. 5d). During that year, the model was advanced without data assimilation except for the input through the RTOFS-Global lateral boundary conditions. Simulations at 1/12° resolution and no data assimilation with HYCOM generally show weaker western boundary current extensions and mesoscale variability than is observed, while both the current magnitude and variability intensify at higher resolution (Haza et al. 2012; Mensa et al. 2013). West of 140°E the small width, high intensity, and defined

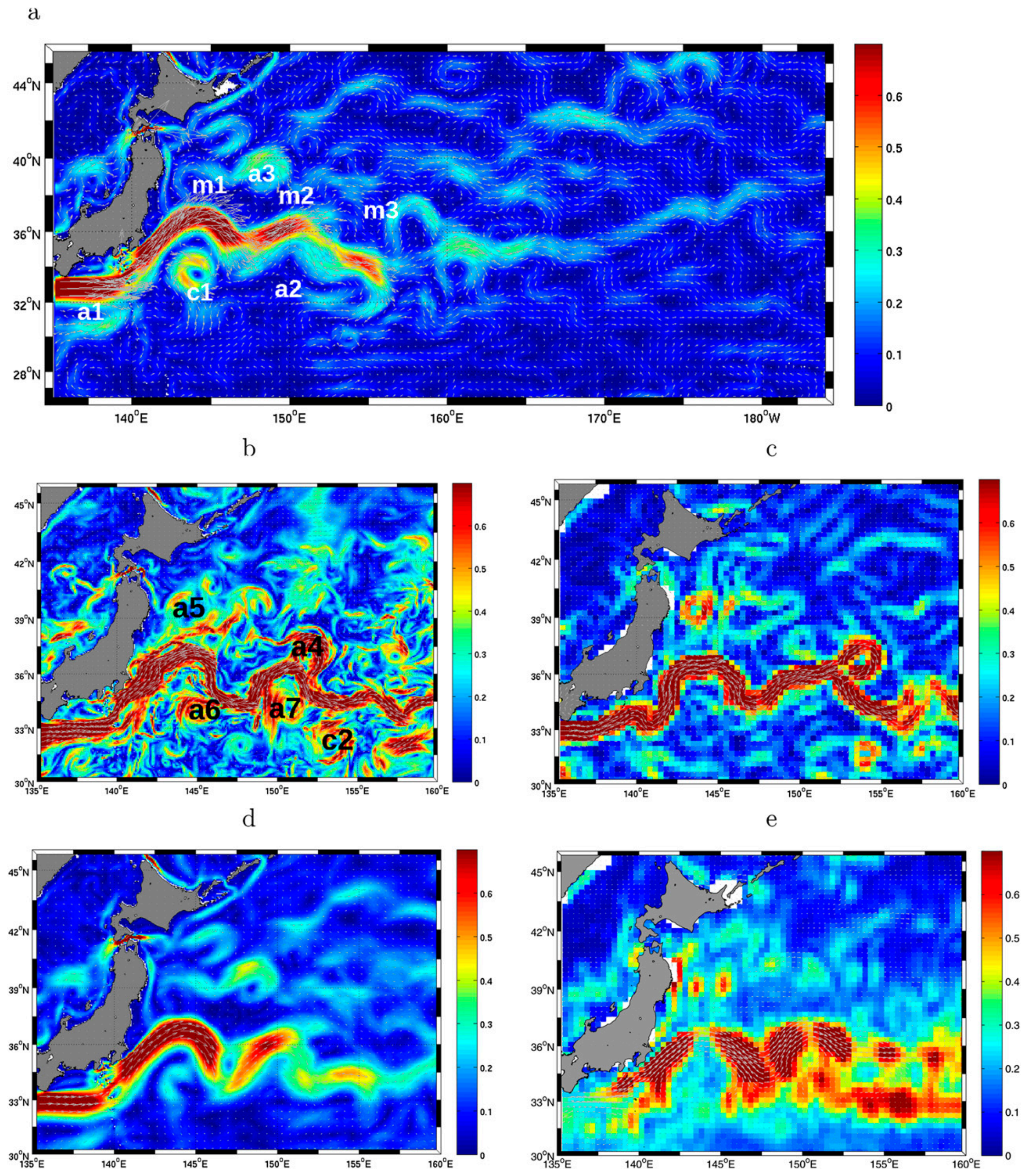

FIG. 5. Velocity and speed (m s^{-1}) (a) simulated as annual mean (May 2011–April 2012) at 15-m depth (depth of drogued in situ drifters) in the region containing the Kuroshio and KE; (b) simulated for 27 Apr 2011 at 0.5-m depth for the region including the Kuroshio and western KE; (c) AVISO geostrophic velocities for 27 Apr 2011; (d) simulated as annual mean (May 2011–April 2012) at 0.5-m depth; and (e) AVISO (geostrophic velocities) as annual mean (May 2011–April 2012). Plotted domains extend to the western model boundary. Indicated in (a),(b) are semipermanent meanders (m1 and m2), meander and deflection (m3), anticyclones (a1–a7), and cyclones (c1 and c2).

TABLE 2. Max surface concentration (Bq m^{-3}) of ^{137}Cs during 25 Apr 2011–15 Dec 2012, location of the max surface concentration, and the total ^{137}Cs amount. The max is listed for the ocean interior; when the absolute max occurs on the coast, its value is listed in parentheses. The ^{137}Cs content over the total volume of the model is 5.4 PBq for 25 Apr 2011 (with atmospheric deposition source), and 10 PBq on and after 27 Apr 2011 (after coastal discharge is added). The absolute max surface concentration (110 000 Bq m^{-3}; not shown) occurred on 31 Mar 2011, with atmospheric deposition source.

Date	Max surface concentration (Bq m^{-3})	Location	Total amount (PBq)
25 Apr 2011	7200	37.8°N, 141.2°E	5.4
27 Apr 2011	10 200	36.8°N, 140.8°E	10
15 Jun 2011	3120	38.1°N, 141.0°E	10
15 Sep 2011	44	40.3°N, 150.5°E	10
15 Dec 2011	22 (33)	40.9°N, 155.0°E	10
15 Mar 2012	14 (24)	40.8°N, 163.8°E	10
15 Jun 2012	9 (16)	43.0°N, 156.2°E	10
15 Sep 2012	7 (10)	40.0°N, 176.4°E	10
15 Dec 2012	7 (8)	41.6°N, 176.2°E	10
15 Mar 2013	6	42.6°N, 178.3°W	10

position of the annual mean modeled Kuroshio indicate that the variability due to Kuroshio path fluctuations (Kawabe 1995; Qiu 2001) is not captured, due to the path fluctuations not having a strong signal at the western model boundary (135°E), and also due to the imperfect nesting (section 2a). Overall, the model starts with a realistic representation of the main currents and eddies, and may initially produce enhanced mesoscale variability. As it evolves, the KE weakens, and weaker than observed variability is produced in the meanders of the Kuroshio and KE.

b. *Tracer evolution*

The horizontal (surface) and vertical tracer distributions close to Fukushima, before and after adding the coastal discharge, are shown in Fig. 4. Adding the coastal discharge, the maximum surface concentration (Table 2) increased from 7200 to 10 200 Bq m^{-3}, and the surface region with highest concentrations (Figs. 4a,b) became more extended to the south and slightly more extended to the east. The southward extension of the tracer is due to a current advecting the discharged tracer in the coastal model (Masumoto et al. 2012). This current is apparent in the simulation before introducing the coastal deposition, but is not well resolved. Eastward extensions of the tracer beyond 142°E result from including the coastal model tracer (Fig. 4b), at 38°N and between 36° and 37°N. The 38°N extension is due to northeastward currents and anticyclonic eddies in NOS-ROMS, while a zone with low velocities and a cyclone are present in RTOFS-ET_WPA between the coast and 143°E. The eastward extensions of tracer between 36° and 37°N are due to fast advection (during 1 day) of the southward extension of the coastal source tracer by the simulated Kuroshio, which is located too close to the coast in RTOFS-ET_WPA (Figs. 5b,c; near 36°N, 141°E). After the addition of the coastal discharge, the ^{137}Cs distribution also extended deeper and had higher subsurface values (141.8°E meridional sections and 36.7°N zonal sections; Fig. 4c,d and 4e,f, respectively).

Vertical and horizontal diffusion parameterization in NOS-ROMS influenced the distribution of the added ^{137}Cs. By using NOS-ROMS for coastal discharge, we introduced a realistic horizontal distribution of the coastal tracer that could not be totally resolved by RTOFS-ET_WPA. However, NOS-ROMS has high vertical diffusion/mixing: RTOFS-ET_WPA, which has KPP mixed layer diffusion parameterization and very low numerical vertical diffusion, produces a tracer patch extending to 500-m depth (Figs. 4c,e), while the NOS-ROMS tracer extends below 1500 m. This is a reason for which the surface tracer concentration in NOS-ROMS is up to 10 times lower than in the observations and other models with similar sources considered by Masumoto et al. (2012). Therefore, low surface concentrations of coastal source tracer are to be expected in our simulation.

The total ^{137}Cs amounts in the HYCOM simulation in the region covered by NOS-ROMS (Fig. 3) were 2 and 6.5 PBq before and after adding the coastal discharge, respectively, while in the entire WPA model domain these amounts for the same times were 5.4 and 10 PBq, respectively (Table 2).

1) MAXIMUM SURFACE CONCENTRATION AND NORMALIZED VERTICAL SLAB TRACER CONTENTS

After the addition of coastal discharge, the model evolved with no extra sources. The maximum surface concentration steadily decreased (Table 2 and Fig. 6). The absolute maximum value of the surface concentration (110 000 Bq m^{-3}; not shown) occurred on 31 March 2011, with tracer from atmospheric deposition only. This quantity quickly declined to 7200 Bq m^{-3} on 25 April 2011 (first row in Table 2). A continuation of the simulation with only an atmospheric source until July 2011 (not shown in this study) showed that without extra sources the maximum value of the surface concentration would have decreased to 1000 Bq m^{-3} on 2 July 2011, that is to <1% of the maximum in 4 months. This is a relatively faster decline than the approximately 7 months reported by Behrens et al. (2012) to reach 1% of

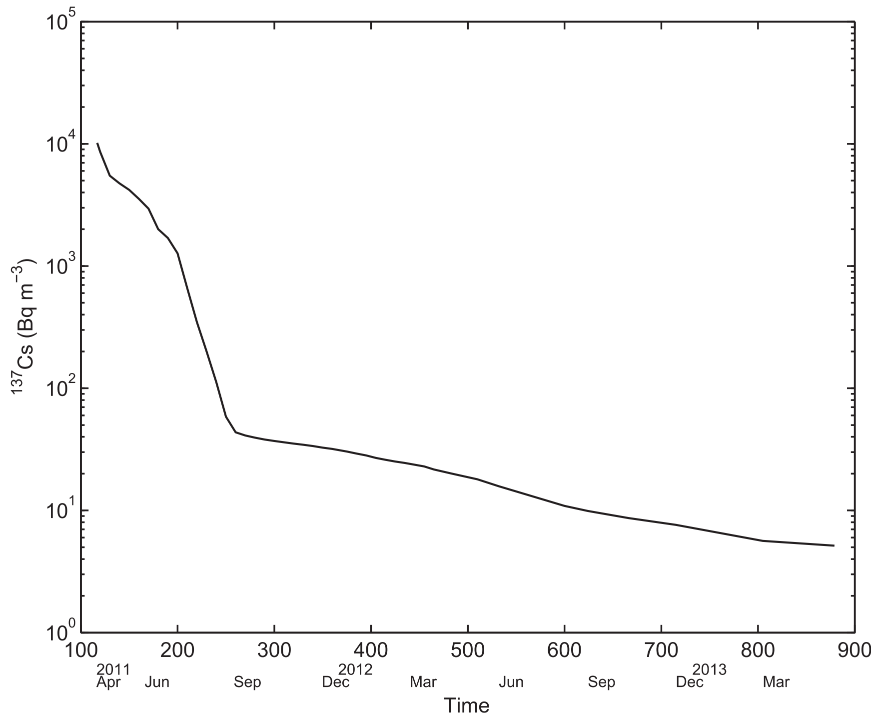

FIG. 6. Max surface ^{137}Cs concentration (Bq m^{-3}) vs time, after 27 Apr 2011, when both atmospheric deposition and coastal discharge were included in the simulation (Julian days since 1 Jan 2011 indicated).

the surface tracer maximum. This difference is expected due to the larger extent of the tracer patch produced by atmospheric deposition versus coastal discharge, immediately reaching eddies located off the coast, together with the Kuroshio and KE that quickly advected and dispersed the tracer. Other differences with Behrens et al. (2012) can be attributed to differences in numerical models and initializations, and also in atmospheric forcings, parameterizations of mixed layer, viscosity, and tracer diffusivity.

The maximum surface concentration (Fig. 6) was 10 200 Bq m^{-3} on 27 April (the initial day with tracer from atmospheric deposition and coastal discharge), and decreased to 110 Bq m^{-3} by August 2011, or 1% of the maximum with both sources, also 4 months after this relative maximum. It reached values below 20 Bq m^{-3} by March 2012, and 6 Bq m^{-3} within 2 yr after the accident, a value that is a few Becquerel above the ~2 Bq m^{-3} background level in the 2000s (Aoyama et al. 2012, 2013). The maximum surface concentration declined with time scales of 40 days for the period of April–July, 20 days for July–August, and a much slower 250 days starting in September 2011.

During most of the simulation period, the maximum concentration remained below levels considered dangerous for human consumers. (The Environmental Protection Agency gives a maximum contamination level for drinking water of about 7000 Bq m^{-3}.)

The tracer content normalized by the total tracer amount (10 PBq) was computed for vertical slabs at 0–100, 100–400, 400–700, 700–1000, and below 1000 m (Fig. 7). The subsurface tracer came from tracer originally deposited at the surface by atmospheric deposition or on the coast through coastal discharge. The tracer content at the surface slab (0–100 m) steadily decreased, while the tracer was transferred to deeper depths, starting with a maximum decrease (April–June 2011, going from 45% to 30% of the total tracer), followed by a slower decrease during the rest of 2011, leveling at 18% in May 2012 and beyond. The subsurface slab for depths of 100–400 m showed a tracer increase initially and then again in September 2011–April 2012 (fall and winter), while there was a slight decrease in summer (July–September 2011). The variations in June–September 2011 (around day 200), and small variations after December 2012 (around day 800), indicate seasonal tracer exchanges with the 0–100-m slab. The tracer in the 400–700-m slab also shows a maximum initial increase, gradually leveling off after February 2012, and the 700–1000-m slab shows an increase, leveling off at the end of 2012. No variations were noticeable for slabs below 1000 m. The initial tracer content for 1000 m–bottom

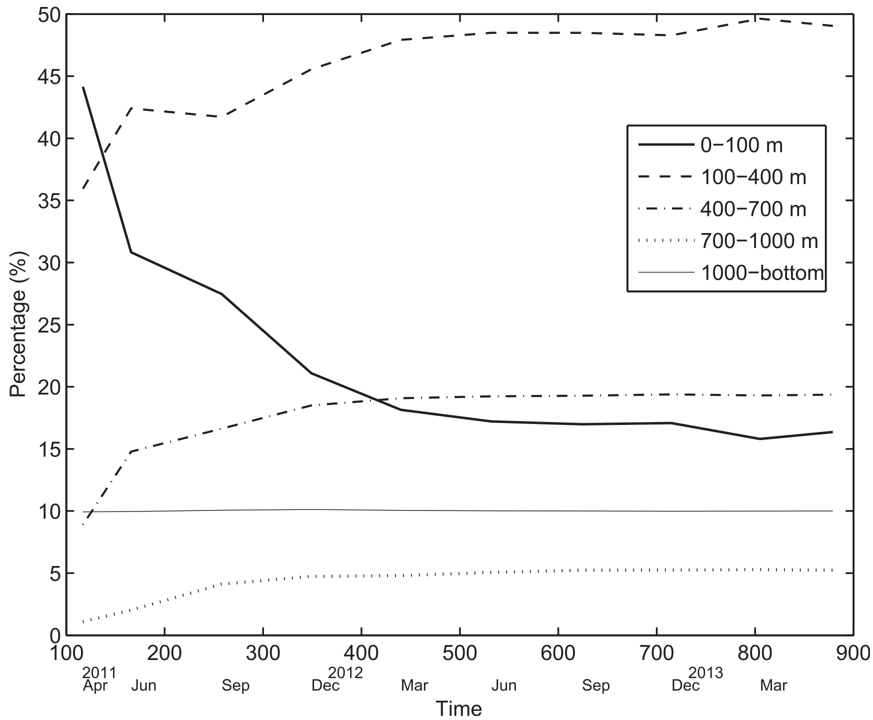

FIG. 7. Mean tracer fraction (%) vs time, computed every 3 months, for depths 0–100, 100–400, 400–700, 700–1000, and 1000 m–bottom (Julian days since 1 Jan 2011 indicated). The total tracer content is constant and equal to 10 PBq.

(10%) resulted from the coastal discharge as provided by NOS-ROMS.

2) VERTICAL SECTIONS

We present results for two model vertical sections at 37.5°N and 150°E (Figs. 8 and 9). A zonal section of the tracer at 37.5°N (Fig. 8) is located north of the Kuroshio through the maximum of the tracer patch for April 2011 (Fig. 4b), but is south of the surface tracer patch maximum for later months [section 3b(3)]. The section shows the tracer evolving toward the east with time, detaching from the coast of Japan, with a concentration modulated by meanders and eddies, and with a subsurface maximum at 200–400 m after June 2012. This maximum is centered at 160°E during June 2012 (Fig. 8e) and at 170°E during December 2012 (Fig. 8f). The tracer is well mixed from the surface to just above the subsurface maximum. For March and August 2013 (not shown) the subsurface maximum in the 37.5°N zonal section can be identified at layers 13 and 14 (σ_2 35.50–36.04, where σ_2 is potential density referenced to 20 MPa), 200–300-m depth, and is located between the northern branch of the Kuroshio and the KE (see Fig. 5a), at 165°E–178°W and 175°E–173°W, respectively. This is the reported location of the light central mode water (LCMW) discussed by Suga et al. (2004) and Oka and Qiu (2012), but the observed LCMW density corresponds more to layer 12 instead of layers 13 and 14.

Meridional sections across the Kuroshio (150°E; Fig. 9) show the upper 400-m tracer limited to the north of the Kuroshio front. The concentration shows a sharp front coincident with the Kuroshio's location for times until December 2011, before the tracer moves east of 150°E. In June 2011, a subsurface tracer maximum is evident at about 600 m (layer 16, σ_2 36.04) at 35°N, a location south of the surface Kuroshio front (37°N). This layer represents in the model the intermediate water (Talley 1993) identified by a salinity minimum in the water column. This subsurface tracer maximum persisted south of the front through the winter and the following summer. For both March and August 2013 (not shown) the 150°E meridional section shows a tracer subsurface maximum for layers 14–16 (σ_2 35.50–36.04), including the intermediate water, at 500–700-m depth for 30°N. This event illustrates the subsidence and ventilation of water masses along the Kuroshio front, influenced by frontal motions and eddies. Further discussion on the subsurface tracer evolution is presented in section 3b(4).

The tracer evolution in our model illustrates a possible pathway across the Kuroshio front, following the diving isopycnals with the intermediate water. More work is needed to assess if this possible pathway is excited, because we have obtained it in a simulation initialized by an observed state, and therefore fast

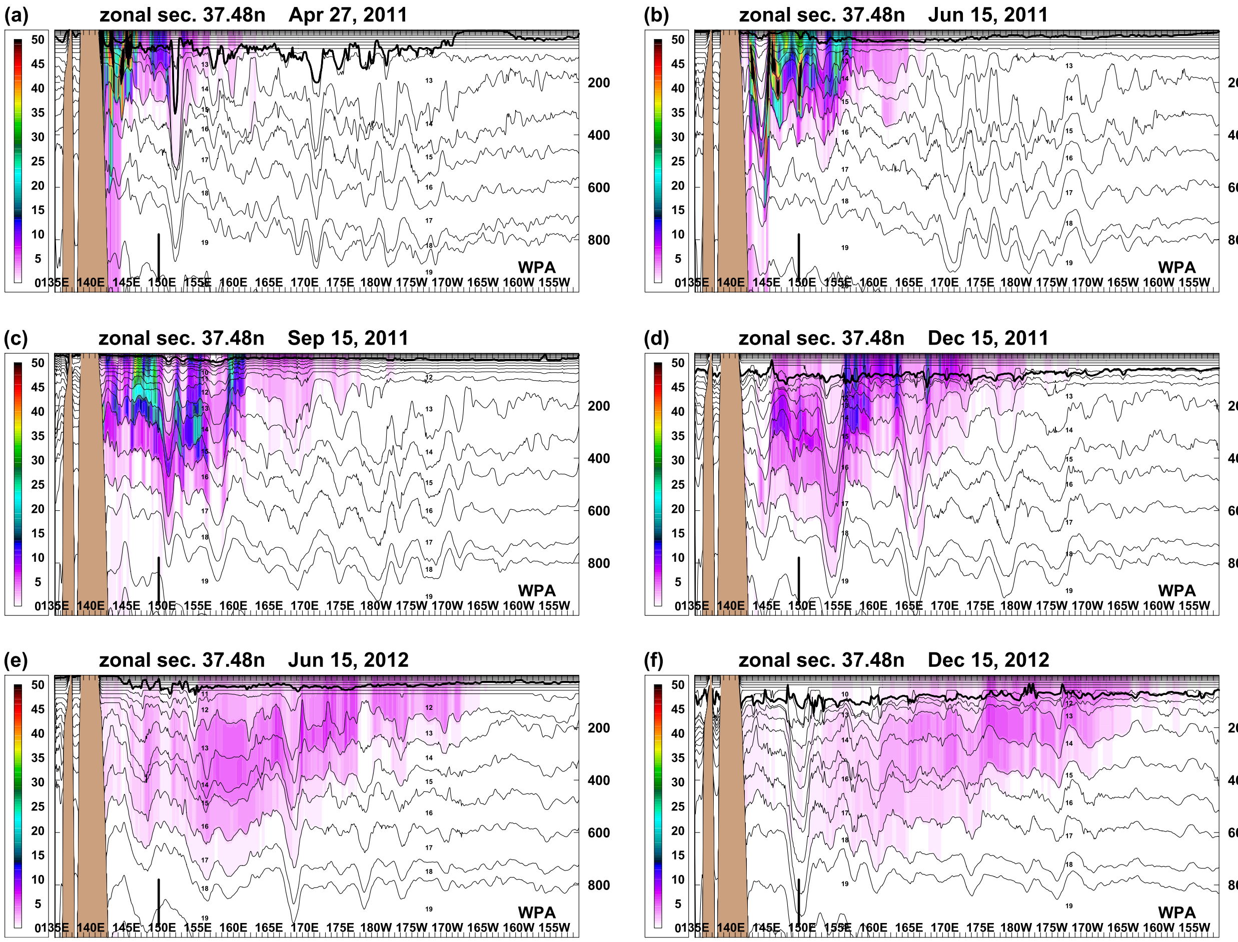

FIG. 8. Simulated ^{137}Cs concentration (Bq m^{-3}) in a zonal section at 37.5°N on (a) 27 Apr 2011, immediately after adding the direct ocean discharge from the coastal model; (b) 15 Jun 2011; (c) 15 Sep 2011; (d) 15 Dec 2011; (e) 15 Jun 2012; and (f) 15 Dec 2012. MLD is indicated by the thick black line. Significant tracer concentrations at depths greater than 300 m near Fukushima after 27 Apr 2011 are mostly due to the NOS-ROMS realization of local coastal discharge. The long tick mark indicates 150°E (lon of the meridional section in Fig. 9).

adjustments toward an equilibrium state are to be expected. The evolution of the subsurface tracer is also sensitive to the kind of surface boundary conditions being of fluxes or including relaxation to surface temperature and salinity. You (2003) and You et al. (2003) discuss the transformation for the North Pacific Intermediate Water in an extended pathway through the Kuroshio–Oyashio mixed-water region and the subarctic–tropical frontal zone, from 140°E to 140°W. Although there are not enough observations to assess if the pathway in the western Pacific found in our simulation was active for the Fukushima tracer, we speculate that part of the tracer may have followed it across the front.

3) SURFACE TRACER EVOLUTION

The atmospheric deposition is quickly distributed through the mixed layer. The simulated mixed layer depth (defined in section 2a) averaged for the first 20 days of the simulation (Fig. 10) generally compares well with the late winter MLD climatology of Suga et al. (2004). A band of MLD greater than 200 m is present around 40°N, extending to 175°E. The warm eddy north of the Kuroshio was in our initial state (see also Fig. 5b, eddy a4). South of the Kuroshio and around 33°N, MLD values of 200–400 m are present, which are higher than the 250 m in Suga et al. (2004). The maximum extent of the region of deep MLD around 40°N occurs on 17 March. Directly east from Fukushima, on 11 March 2011 (the day of the model initialization from RTOFS-Global), the model MLD has values of about 40 m. Tsumune et al. (2013) pointed out that this value is larger than the 10 m estimated by Estournel et al. (2012) from observations. The MLD increases in the first 70 km offshore to about 200 m due to eddies and fronts off the coast.

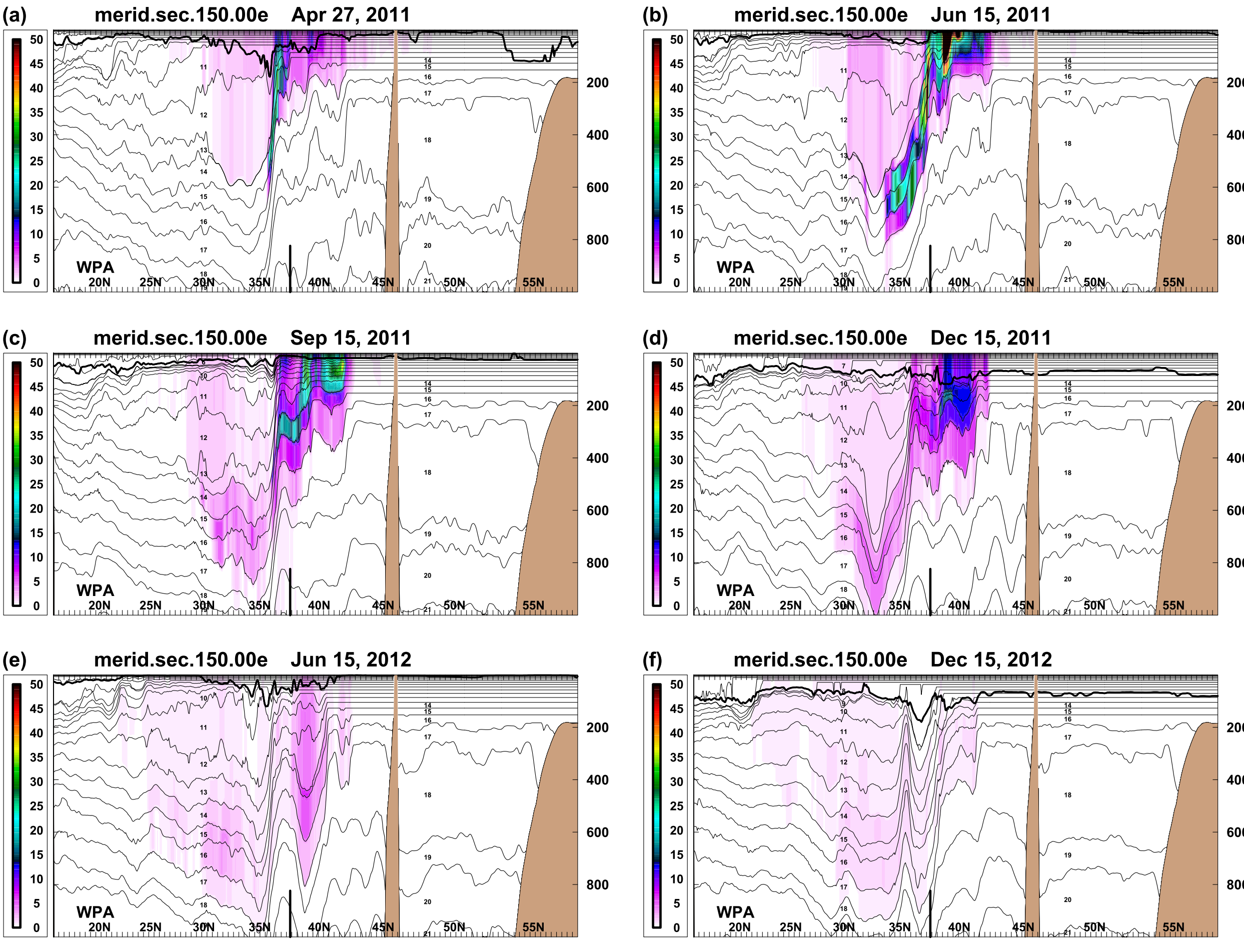

FIG. 9. As in Fig. 8, but for a meridional section at 150°E. Noticeable is the penetration of the tracer along the isopycnals near the Kuroshio front, and subsided tracer south of the front after 15 Jun 2011. The long tick mark indicates 37.5°N (lat of the zonal section in Fig. 8).

We have compared our time mean MLD for 11–31 March 2011 with those from both RTOFS-Global and Naval Research Laboratory/Naval Oceanographic Office (NRL/NAVOCEANO) GOFS hindcasts (www.hycom.org; not shown). This last simulation includes the most recent data in their daily data assimilation (RTOFS-Global is initialized from NAVOCEANO's hindcast of 2 days prior to the present; see appendix B). The maximum MLD in NAVOCEANO's hindcast is 245 m, in good agreement with climatology. The MLD from RTOFS-ET_WPA has a similar horizontal distribution when compared to that of NAVOCEANO's hindcast, but is deeper. The ratio between the MLD from RTOFS-ET_WPA and NAVOCEANO is 1.5–2 for the regions of MLD larger than 240 m in Fig. 10.

Horizontal surface currents (the Kuroshio and KE) contributed to a dilution of the surface ^{137}Cs concentration. The surface concentration of ^{137}Cs (Fig. 11, initial dates also shown in logarithmic scale in Fig. 12) produced a tracer patch that evolved by moving to the east with the currents north of the Kuroshio and Kuroshio Extension, and dispersed within the rich mesoscale eddy structure of the KE. The maximum tracer concentrations occurred north of the Kuroshio, with the current acting as a barrier for the tracer (clearly shown in Fig. 11), in agreement with observations by Buesseler et al. (2012) and modeling studies (Behrens et al. 2012; Rypina et al. 2013).

West of 160°E, the surface tracer was located north of the Kuroshio front (15 June and 15 September 2011; Figs. 11b,c). On 15 September 2011 (Fig. 11c), the tracer was also mostly limited to the north of the KE northern branch between 160° and 170°E, with some tracer leaking into the KE southern branch around 35°N, while a current breaking off north of the northern branch is present at 165°E–180° (with approximately 5 Bq m^{-3} concentrations). The surface tracer located to the north of the front (listed as a fraction of the total surface tracer

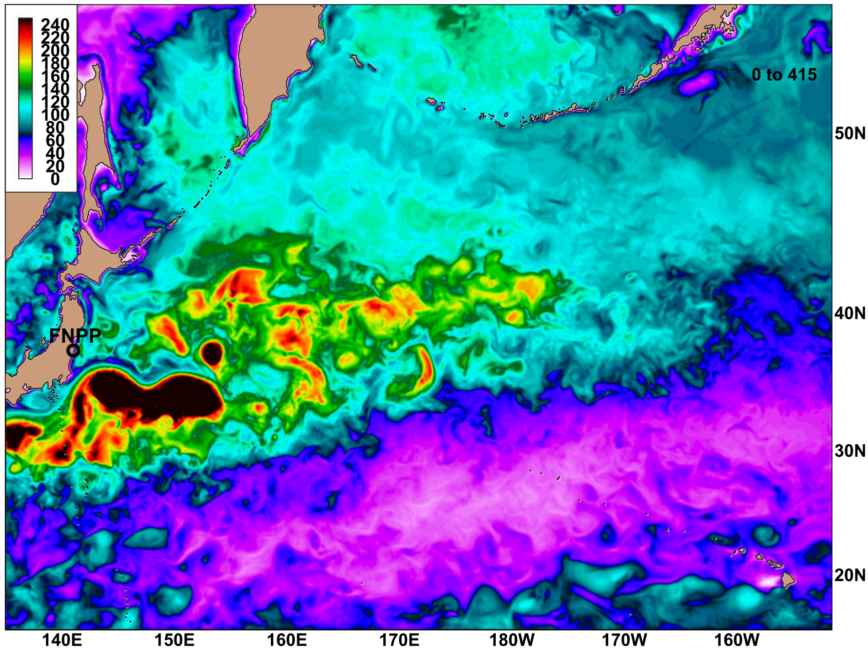

FIG. 10. Model MLD (m), time mean of daily values for 11–30 Mar 2011. The max occurs south of the Kuroshio (34.3°N, 145.7°E; values greater than 400 m extend less than 100 km around this point); the eddy north of the front has an MLD of about 350 m. The FNPP location and the min and max values of the shaded field are indicated.

in Fig. 11) was identified as being collocated with values of SSH smaller than 0.3 m, except for the eddy at 33°N, 145°E, in Fig. 11c, which contributed 2% to the surface tracer to the south of the front. The fraction of surface tracer to the north of the front decreased from 0.94 to 0.58 during the 600 days of the simulation in Fig. 11. As in Behrens et al. (2012), the presence of larger proportions of tracer in the recirculation region to the south of the Kuroshio Extension occurred when the tracer patch reached locations in the central Pacific where the front was less pronounced, as found east of 160°–165°E for 15 September and 15 December 2011 (Figs. 11c,d). Cyclonic cold-core rings that formed and pinched off the KE contained relatively high tracer amounts, transported tracer south of the KE, and later moved westward in the recirculation region south of the Kuroshio and KE. From a meander of the Kuroshio (Fig. 11b; 15 June 2011, 35°N, 147°E), a ring containing tracer detached on 14 July 2011, stayed near that longitude through 15 September 2011 (33°N, 144°E; Fig. 11c), then moved westward and was reabsorbed by the Kuroshio by the end of October 2011 (movies are available online at http://polar.ncep.noaa.gov/global/tracers/, with the WPA region labeled as WPAb). The small regions of tracer-relative minima on the north side of the Kuroshio front for 27 April 2011 (Fig. 11a), at 36°N, 152°E (eddy a4; Fig. 5b), and 36°N, 157°E, corresponding to anticyclonic warm-core eddies on the north side of the front, also originated in the KE. The surface tracer for 15 June and 15 December 2012 (Figs. 11e,f) shows a more mixed tracer field, and a tracer maximum concentration of 8 Bq m^{-3}, or about 4 times the pre-Fukushima maximum concentration. For March and August 2013 (not shown) the maximum surface tracer has values of 6 and 5 PBq, respectively, and the tracer patch is approximately distributed around 41°N, 180° and 40°N, 170°W, respectively.

4) SUBSURFACE TRACER EVOLUTION

Behrens et al. (2012) discussed how from the initial time of their simulation, at a time of deep mixed layer depths at the end of the winter, the tracer penetrated through O(200 m)-deep convection along the Kuroshio in the western North Pacific due to wintertime cooling (Suga et al. 2004), resulting in a rapid penetration of the tracer to 500-m depths in the first weeks of the simulation.

In our model, at 400-m depth, the tracer initially appeared on the Kuroshio front (represented by the 35.2-σ_2 density line; see Fig. 13a, 27 April 2011), with some tracer leaking to the south. Local atmospheric deposits occurred in the region around 34°N, 145°E, where the March 2011 model MLD was ≈400 m and where the atmospheric source can contribute 2–5 Bq m^{-3} over the

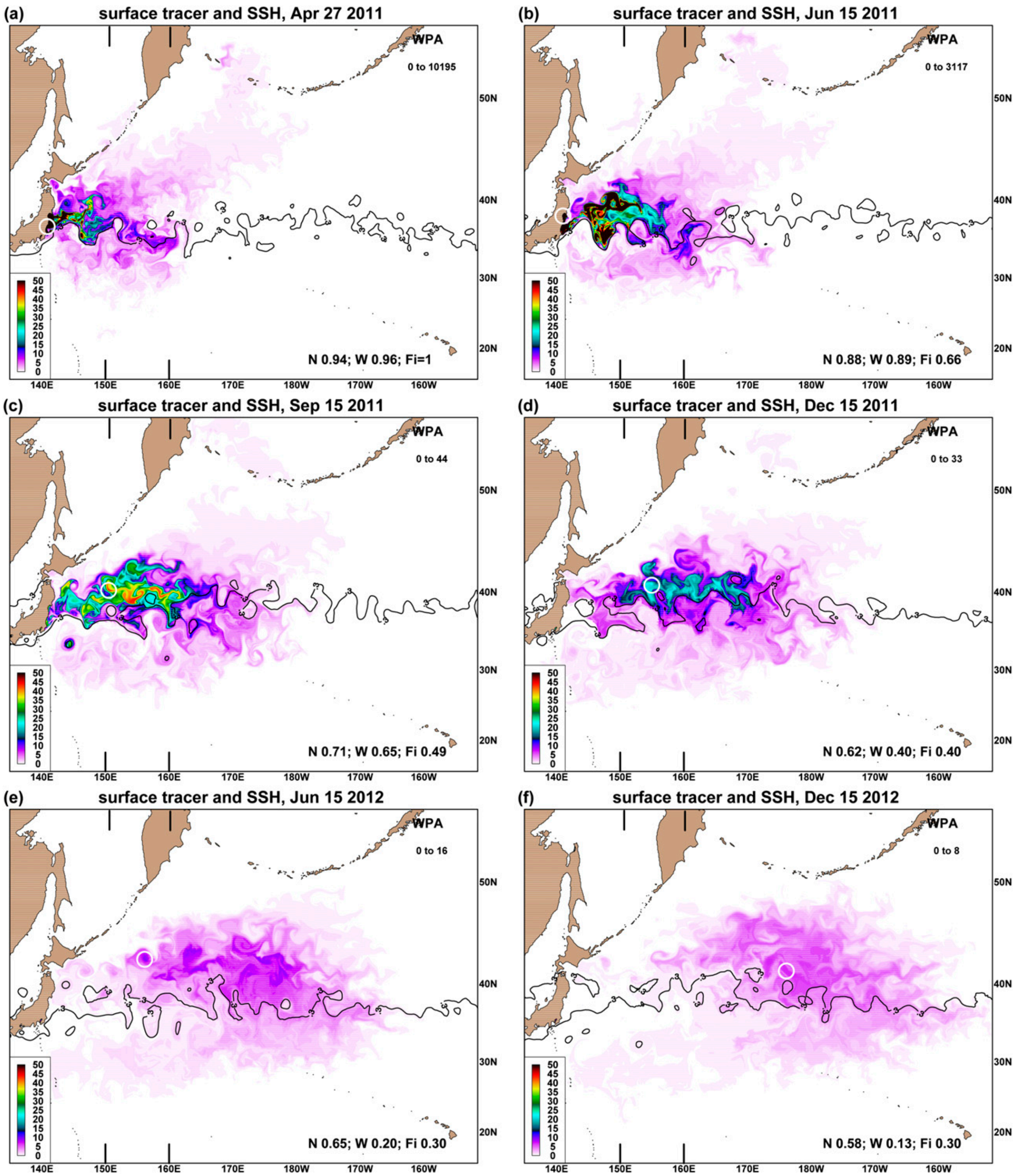

FIG. 11. Simulated surface ^{137}Cs concentration (Bq m^{-3}; color shaded), for the dates in Fig. 8. The Kuroshio–KE front is indicated by the 0.3-m contour of the model instantaneous SSH, along with the fraction of the surface tracer to the north of the front (N), west of 160°E (W), and the total surface tracer as a fraction of its value on 27 Apr 2011 (Fi), as well as the min (0) and max of the shaded field. White circles indicate the locations of the surface tracer maxima (Table 2). Long thick tick marks indicate 150° and 160°E [sections 3b(2) and 3b(3)].

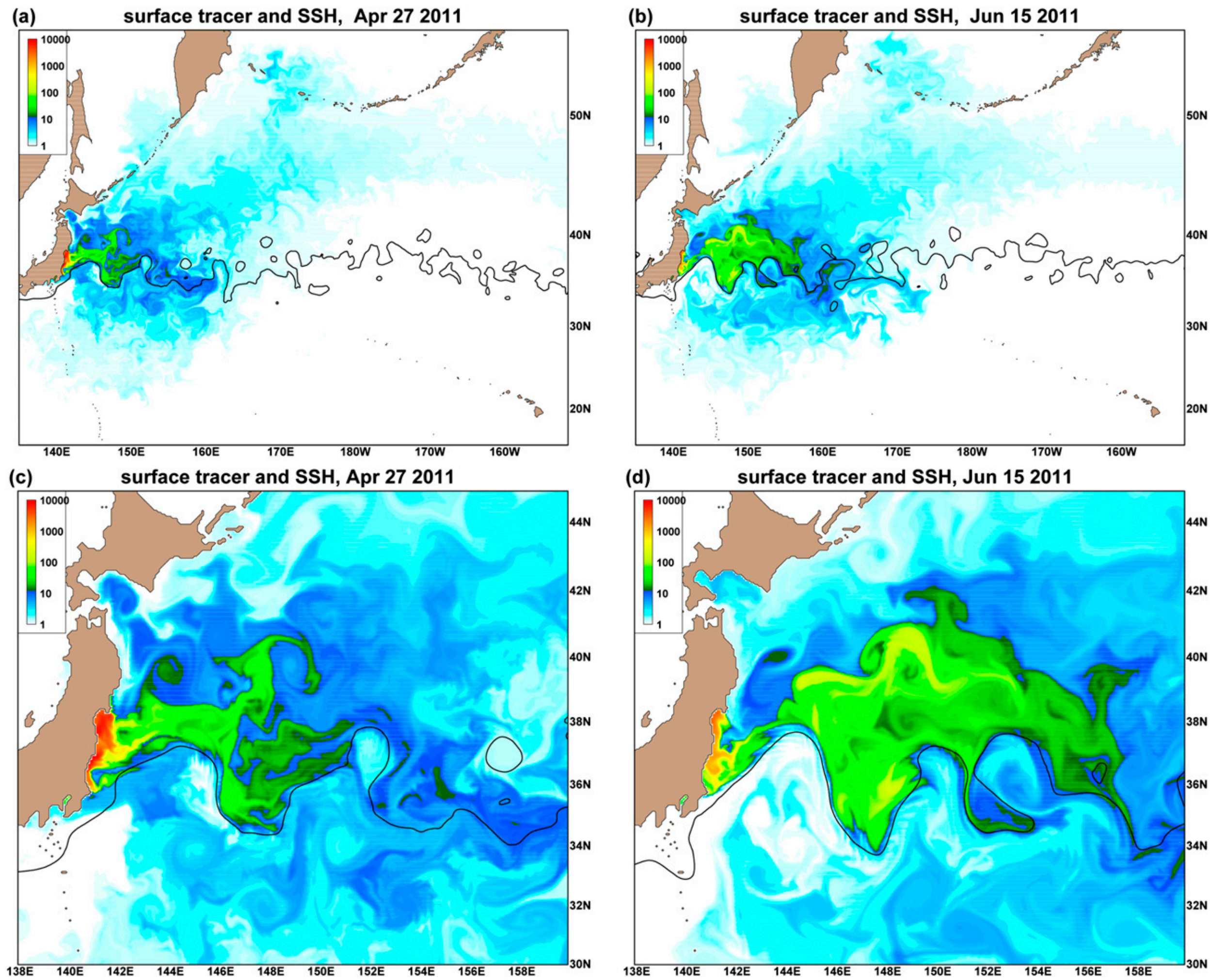

FIG. 12. Simulated surface ^{137}Cs concentration (Bq m^{-3}) on logarithmic scale for the total model domain and 0.3-m SSH contour: (a) 27 Apr and (b) 15 Jun 2011. (c),(d) As in (a),(b), but for details near Fukushima–Daiichi on 27 Apr and 15 Jun 2011, respectively.

mixed layer. The patch near the coast west of 145° was introduced by NOS-ROMS. Figure 13a is the subsurface counterpart to Fig. 4b, and is the horizontal representation of the 400-m concentrations seen in Figs. 4d and 4f. The cyclonic eddy located at 33°N, 144°E, on 15 September 2011 (Fig. 13c) can be seen as a relative tracer maximum at 400 m, its cold core reaching 400 m but not 700 m (Fig. 14c). The 400-m tracer generally moved to the east, but at a slightly slower pace than the surface tracer, due to weaker subsurface than surface currents [quantified later in section 3b(5)].

The distribution of the 400-m tracer is consistent with tracer passing through the region of central mode water (CMW) and LCMW discussed by Suga et al. (2004), Oka and Suga (2005), and Oka and Qiu (2012), and with the tracer evolution in Behrens et al. (2012).

At 700-m depth the tracer remained mostly located south of the front (represented by the northern branch of the 36.0-σ_2 density line), at all times (Fig. 14). A comparison with a simulation with atmospheric deposition only (not discussed here) showed that most of the June 2011 tracer at 700 m (Fig. 14b) resulted from coastal discharge as provided by the NOS-ROMS coastal model and is probably unrealistic, but in terms of horizontal distributions, the 700-m tracers from coastal discharge and from atmospheric deposition were similar. The passage of tracer toward the southern part of the front at depths larger than 500 m is illustrated in Fig. 15, showing the tracer horizontal distribution at layer 16 (with nominal density σ_2 36.04). Figure 15 is the layer 16 counterpart of the 150°E section of Fig. 9b. The tracer penetrates south of the front in the western part of the first southward meander of the Kuroshio (33°–35°N,

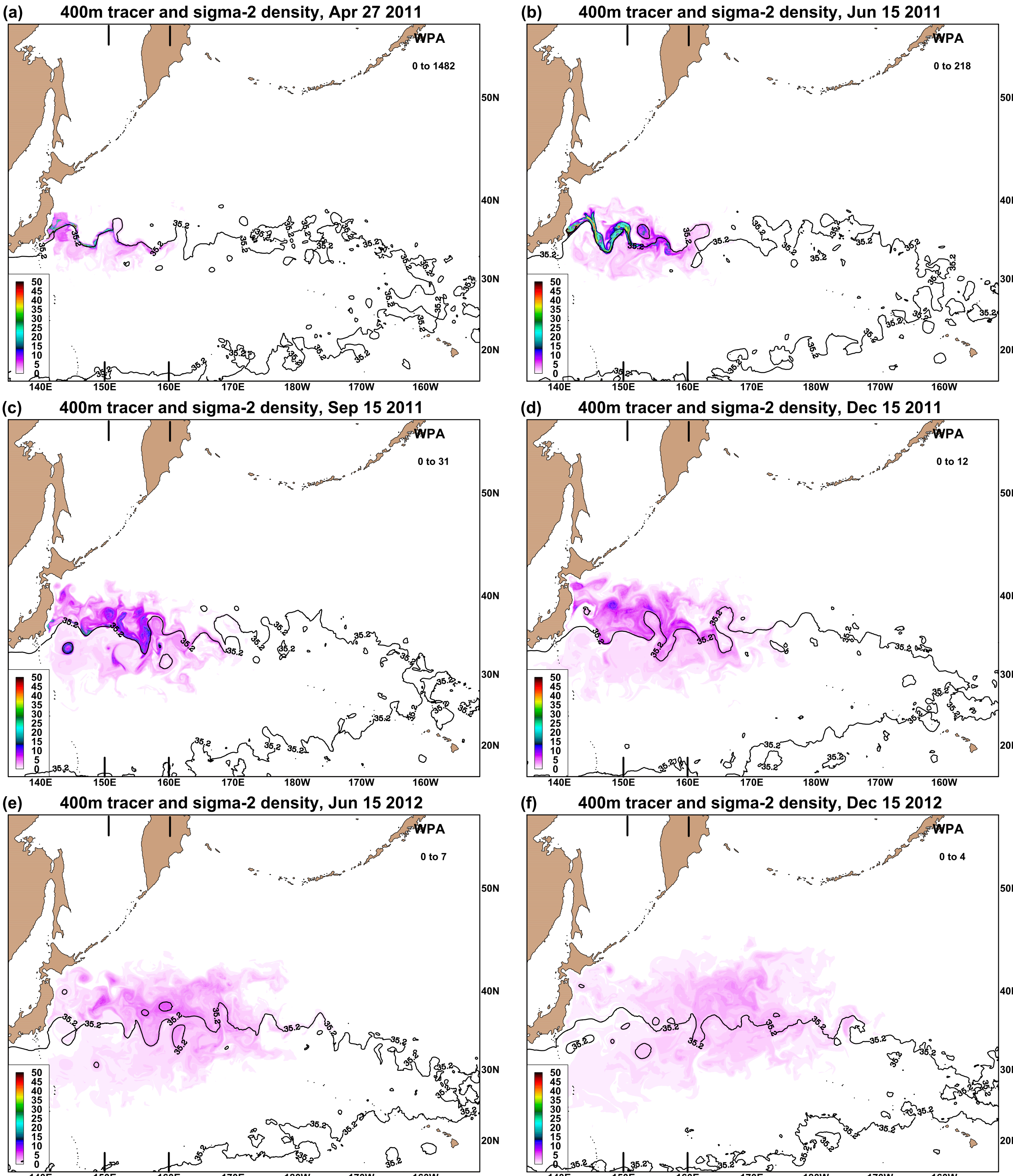

FIG. 13. Simulated ^{137}Cs concentration (Bq m^{-3}) at 400-m depth, and 35.2-σ_2 density line, for the dates in Fig. 8.

145°–146°E; m1 in Fig. 5a), and on the second southern meander (32.5°–35°N, 150°E; m2 in Fig. 5a). As discussed in section 3b(2), tracer from the north of the Kuroshio front penetrates southward along the isopycnals, below the warm subtropical water pool. Instabilities also seem to contribute to the southward transport of tracer near the front (Pollard and Regier 1992; Follows and Marshall 1994; Marshall 1997).

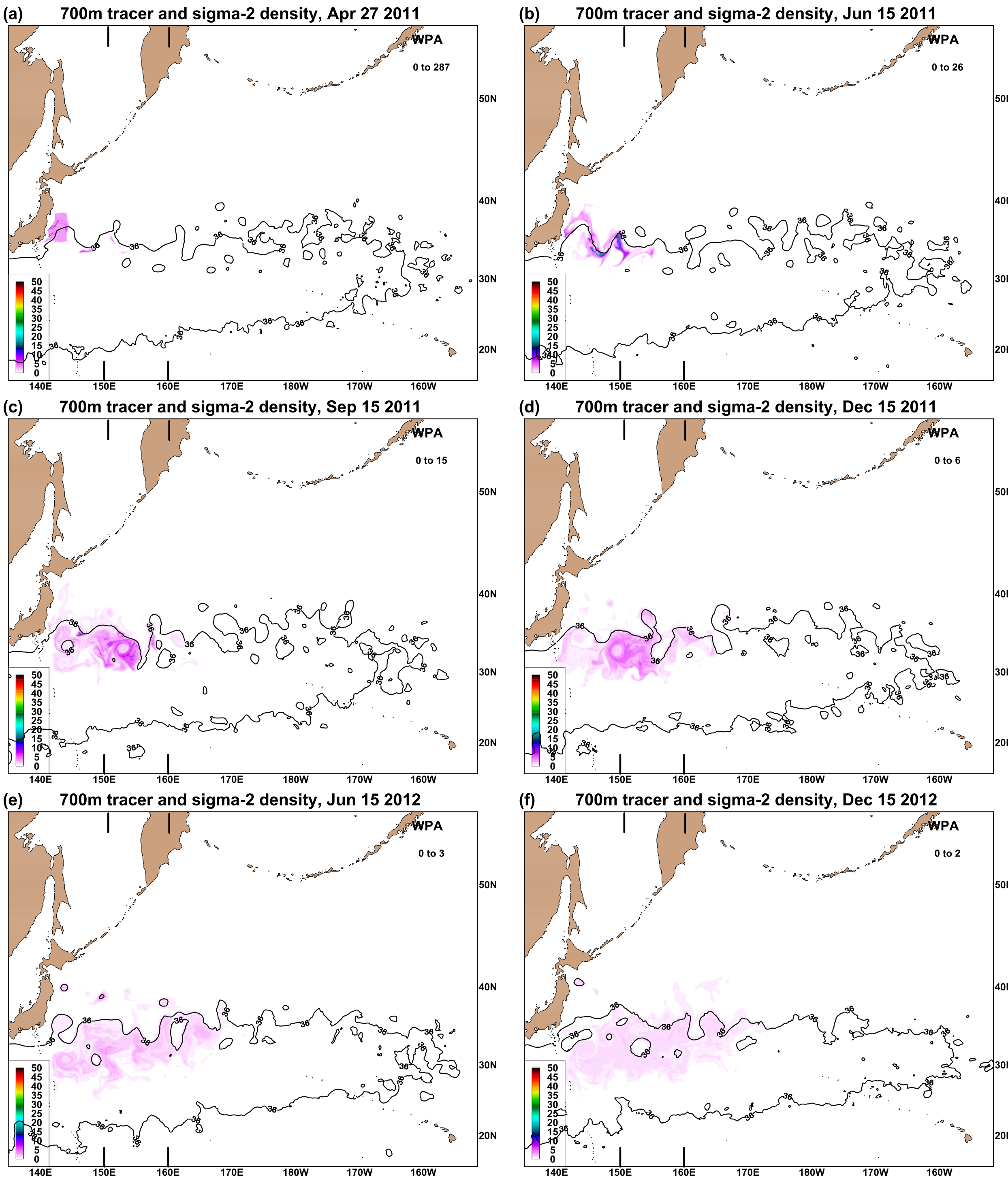

FIG. 14. Simulated ^{137}Cs concentration (Bq m^{-3}) at 700-m depth, and 36.0-σ_2 density line, for the dates in Fig. 8.

In summary, the tracer tends to stay to the north of the Kuroshio front for depths to which the Kuroshio front penetrates as a strong front, and is south of the front below those depths. Winter vertical mixing in the mixed layer, central mode water formation north of the Kuroshio front, along-isopycnal mixing near the Kuroshio front, eddy transports, and southward transport with the lower part of the Pacific subtropical meridional cell at

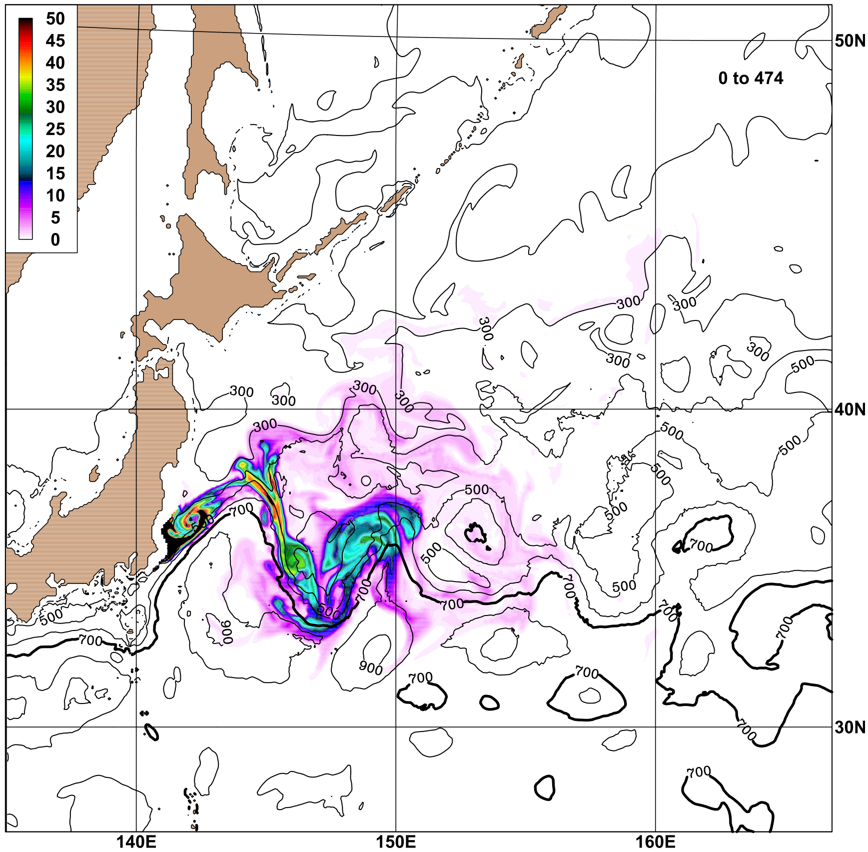

FIG. 15. Tracer concentration (Bq m^{-3}; color shaded) and layer depth (m; contoured) for model layer 16 (with nominal density σ_2 36.04), for 15 Jun 2011. The 700-m depth is marked with a thick contour line.

the base of the warm water pool with the intermediate water (Talley 1993), all contribute to the redistribution of the tracer toward deeper depths.

5) TRACER CENTER OF MASS

The tracer center of mass moved mostly eastward (Fig. 16): at the surface the motion was eastward with a slight northward component changing to eastward after December 2011, reaching 178°E in December 2012 (Fig. 16a). The tracer center of mass moved eastward at 400 m, reaching 164°E (Fig. 16b), and moved southeastward (and south of the annual mean front), at 700 m reaching 155°E (Fig. 16c), for the same date.

The horizontal extents of the tracer patch, as indicated by the standard deviation of the tracer distance to the center of mass (not shown), were 560 km for the surface, 450 km for 400-m depth, and 250 km for 700-m depth on 27 April 2011. These standard deviations approximately doubled for the surface, tripled for 400-m depth, and quadrupled for 700-m depth, from 27 April 2011 through 15 December 2012. The eastern boundary of the surface tracer patch, 1 yr after the accident (not shown), with values of about 5 Bq m^{-3}, reached approximately 175°W, and for December 2012 (1.8 yr after the accident) reached 160°W (Fig. 11f). This evolution of the surface distribution is approximately consistent with Behrens et al. (2012).

6) COMPARISON WITH AVAILABLE OBSERVATIONS, AND MODEL UNCERTAINTIES AND ERRORS

The model surface tracer concentrations are compared with Buesseler et al. (2012) observations for June 2011 (Table 3). The observations show values of about 1–3 Bq L^{-1} (1000–3000 Bq m^{-3}) near 36.5°N, 142°E; values of 20–800 Bq m^{-3} south of 38°N and west of 143°E; and values of about 100 Bq m^{-3} south of 38°N and at 144°–147°E.

In the model, on 15 June 2011, the tracer is more concentrated near Japan, and the model values are lower than observed, by a factor of 5 for the average at all of the observed locations (not shown). Selected observed and modeled concentrations are given in Table 3: the modeled tracer has values of about 300–1100 Bq m^{-3}

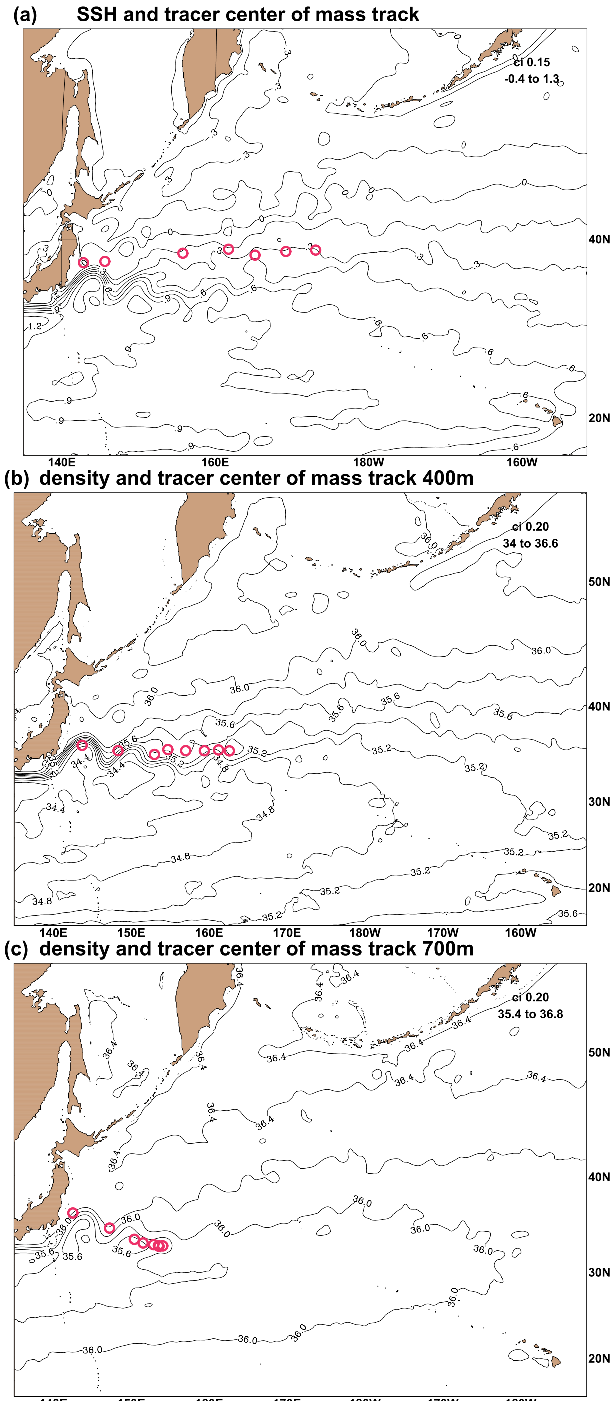

FIG. 16. Evolution of the position of the center of mass of the tracer, for the following dates: 27 Apr 2011, 15 Jun 2011, and every 3 months afterward until 15 Dec 2012. The centers of mass positions (circles) are superimposed on annual mean May 2011–April 2012 fields (contour lines) of (a) SSH (m) for the surface tracer and σ_2 density for the (b) 400- and (c) 700-m tracers. Successive times correspond to successive eastward locations as the center of mass moves always to the east. The contour interval (ci), and max and min of the contoured field are indicated.

near 36°–37°N, 141.4°E; values of 12–130 Bq m^{-3} at 36.2°–37.5°N and west of 143°E; and values of 10–70 Bq m^{-3} south of 38°N and at 144.4°–147°E. Lower model concentrations with values of 0.1–1 Bq m^{-3}, not included in the model points in Table 3, are present near 36.5°N, 144°E. Earlier, in April 2011, the model shows values of 1000–3000 Bq m^{-3} near 37.5°N, 142°E, and values of 30–50 Bq m^{-3} at 38°N and 144°–147°E (see also Figs. 12c,d).

The differences from Buesseler et al. (2012) suggest that better agreement would be achieved if the coastal source was more intense, and had a distribution more extended toward the north and east, similar to those reported in the simulations by Kawamura et al. (2011), Tsumune et al. (2012), or Tsumune et al. (2013), which would produce tracer concentrations closer to the observations in many details. We notice that in their simulations Rypina et al. (2013) found that a coastal source totaling 16.2 PBq better fit the observations, which is a source about 4 times more intense than ours. In addition to vertical diffusion, the surface tracer distribution is influenced by winds, modeled currents, and eddies, which were first represented through NOS-ROMS and then through RTOFS-ET_WPA. Farther offshore at 147°E, the modeled tracer concentration is less than the observed values north of 35.5°N, but greater than the observed values at 34.5°–35.5°N, suggesting that the modeled Kuroshio meander, at that longitude, was about 100 km southward with respect to the observed location. This error is to be expected since the model is not constrained by data assimilation. In addition, a more intense and extended atmospheric deposition can improve the agreement at that longitude a few degrees north of the KE, since in our simulation during June 2011 both coastal and atmospheric sources contribute in approximately equal amounts to the tracer values at 38°N and at 147°E. This is different from what is stated in Rypina et al. (2013), who report that their concentrations at the observed locations and times are almost entirely due to direct oceanic discharge.

To assess the accuracy of the atmospheric deposition source, the model tracer distribution was compared with observations in Aoyama et al. (2012) (Table 4, location numbers 1–5, observations indicated in Fig. 2a). We compare these observations with the 1 April model values (with atmospheric deposition source), when the surface tracer concentration is very close to the total local deposition divided by the mean mixed layer in Fig. 10. In addition we list the concentrations c^* that we estimate would be obtained in a simulation with the NAVOCEANO hindcast MLD, in the following way: c^* is equal to our concentration multiplied by the ratio between our MLD and the NAVOCEANO hindcast

TABLE 3. Observed surface concentrations during June 2011 (Buesseler et al. 2012) and model values, grouped by regions and values. Min and max values for each group are listed. Parentheses in the ''Concentration'' column contain the means over the group of points; only observed values north of the Kuroshio front were taken.

Obs			Model		
No.	Location	Concentration (Bq m^{-3})	No.	Location	Concentration (Bq m^{-3})
5	≈36.5°N, 142°E	1653–3833 (2727)	5	36°–37°N, 141.4°E	336–1147 (639)
23	36.3°–38°N, 141.4°–143°E	23–856 (431)	11	36.2°–37.5°N, 141.4°–143°E	12–130 (54)
9	35.5°–38°N, 144°–147°E	74–329 (146)	10	34.5°–38°N, 144.4°–147°E	10–70 (39)

MLD, both averaged during 11–31 March 2011 [see section 3b(3)]. For the average of all locations (1–8) in Table 4, our modeled MLD is deeper by a factor of 2.5 than that of NAVOCEANO's hindcast. Observed values of 500 and 1000 Bq m^{-3} at the end of March and beginning of April 2011 are reported at about 300 and 600 km, respectively, off Fukushima at approximately 36°N, 144°–147°E (location numbers 1 and 2; Table 4). A contribution of direct discharge at those locations can be present, but our model of coastal discharge and the models in Masumoto et al. (2012) show these values constrained to the west of 141.5°E. The first point (location 1) is located south of the Kuroshio front, as in the observation-based simulation in Rypina et al. (2013), while the second point (location 2) is north of the front. Model concentrations are 12 and 13 Bq m^{-3}. Modified concentrations that would be obtained with the NAVOCEANO hindcast MLD are still much lower than the observed values at those two locations. With our atmospheric source, modeled values of 1000 Bq m^{-3} are found west of 142°E and values of 100 Bq m^{-3} are found at 37°–38°N and west of 145°E. Surface tracer concentrations from HYSPLIT atmospheric deposition are listed together, where possible, with values approximated from the published figures of Stohl et al. (2012) and Estournel et al. (2012). As noted in Table 4, values from HYPSLIT are significantly lower than those from Stohl et al. (2012) at locations 1 and 3. For a scale analysis, we consider the modified concentrations. If for those locations we would assume the use of the atmospheric deposition of Stohl et al. (2012), and in addition the NAVOCEANO hindcast MLD, approximate values (second value in parenthesis for source b at locations 1 and 3) are close to but higher than the observed values (Aoyama et al. 2012). This indicates that HYSPLIT severely underestimates (by a factor of about 20) the atmospheric deposition at those locations, where Stohl et al. (2012) show a band of high deposition. Using the c^*, the best fit for locations 1 and 3 would be obtained with the values in Stohl et al. (2012) divided by 1.5. The model shows negligible concentrations near the date line where ≈200 Bq m^{-3} were observed in May 2011 (Aoyama et al. 2013). According to Kamenik et al. (2013), values of 10 Bq m^{-3} in this region would require atmospheric deposition of 500–1000 Bq m^{-3}, which is not present in our source. A comparison with the measurements in Honda et al. (2012) with values larger than 100 Bq m^{-3} is shown in Table 4 (locations 6–8, indicated in Fig. 2a). For those points, the modeled concentrations are about a third of those observed. Instead, by using the modified concentrations with the NAVOCEANO hindcast MLD, we find good agreement, resulting in the average for the observed concentrations being 1.2 times that of the modified model.

The mean concentration from the observations in Aoyama et al. (2013) prior to the end of May 2011 is 46 Bq m^{-3}, for the 85 observations in the model domain. Model values with no direct discharge, sampled at the observed points over three dates in April–May result in a mean of 6 Bq m^{-3} or a factor of 8 weaker.

We can compare our solution to the observation-based solution presented by Rypina et al. (2013). The eastward extents of the tracer patch over the Kuroshio on 27 April and 15 June 2011 (Figs. 12a,b) are 165° and 170°E in our model, and 170° and 175°E (1 May and 16 June 2011) in Rypina et al. (2013).

Given the considerable uncertainty in sources affecting all modeling efforts, we consider this simulation successful as it has provided further insight into the dynamics governing the pathways and mixing of Fukushima contamination. Uncertainties due to model resolution, model formulation, thermodynamical and mechanical forcing, and parameterizations all contribute to errors in the modeled tracer solutions. However, uncertainties in the strength of the sources seemed to have had the most significant contribution to the overall uncertainty in the estimated tracer inventories.

4. Summary

In response to the Fukushima disaster, NOAA/NCEP was tasked with the responsibility of providing actionable information to the Department of Energy and decision makers in the U.S. government through an Interagency Working Group, with the purpose of separating ocean areas safe for human activity from

TABLE 4. Observed surface concentrations (Aoyama et al. 2013) with values >100 Bq m^{-3} in March–May 2011, and modeled values for April 2011 with only atmospheric deposition: observation source and date, observation number in our table and observed location (see also Fig. 2a), observed surface ^{137}Cs concentration (Bq m^{-3}), model date, modeled surface concentration (Bq m^{-3}; in parentheses for locations 1–4 modeled range in a ~200-km radius region around the location), and approximate c^* that would be obtained with the NAVOCEANO GOFS hindcast MLD (see text). For observations 1–5, total atmospheric deposition (Bq m^{-2}) according to sources (a) HYSPLIT in this analysis and approximated values from (b) Stohl et al. (2012) and (c) Estournel et al. (2012); shown in parentheses are the concentrations that would be obtained by replacing our source with Stohl et al. (2012), and the c^* that would result using the source from Stohl et al. (2012) and the NAVOCEANO hindcast MLD, listed only when Stohl et al. (2012) would improve the agreement with the observation. In comparison with the observations of Honda et al. (2012), the model for 15 Apr 2011 does not contain direct discharge (7 Bq m^{-3} of direct discharge are contributed on 27 Apr to observation 8).

	Obs			Model			Source		
Source	Date	Location	Concentration (Bq m^{-3})	Date	Concentration (Bq m^{-3})	Concentration c^* (Bq m^{-3})	a (Bq m^{-2})	b [Bq m^{-2} (Bq m^{-3})]	c (Bq m^{-2})
Aoyama et al. (2012)	31 Mar	1) 35.68°N, 143.77°E	546	1 Apr	12 (12–300)	25	3542	100 000 (370; 770)	5000
	1 Apr	2) 36.60°N, 147.60°E	1080		13 (10–20)	22	1409	1000	1000
	4 Apr	3) 34.33°N, 144.68°E	181		7 (7–20)	13	1819	50 000 (190; 350)	1000
	4 Apr	4) 34.51°N, 148.40°E	118		5 (5–20)	10	924	—	—
	12 May	5) 42.86°N, 179.60°E	196		0.1	0.1	15	100	—
Honda et al. (2012)	14 Apr	6) 37.86°N, 143.31°E	284	15 Apr	69	183	—	—	—
	15 Apr	7) 38.21°N, 143.79°E	148		79	196	—	—	—
	16 Apr	8) 38.11°N, 143.08°E	174		35	93	—	—	—

potentially threatened areas, in near–real time, and using available resources. Initially this information was provided by using particle-tracking methods, for which essential collaborations were established with the U.S. Navy, NOAA/ARL for their HYSPLIT results, and the Environmental Protection Agency (EPA) in establishing contamination guidelines. A concept of operations [CONOPS, appendix B in Tolman et al. (2013)] was later developed for this part of the project.

The initial approach was then replaced with a fully operational eddy-resolving tracer dispersion model for the region of the northwestern Pacific Ocean (RTOFS-ET_WPA). In this model, the ^{137}Cs concentration has been simulated in the western Pacific with real forcing, in a regional eddy-resolving model initialized from a global eddy-resolving hindcast. The ^{137}Cs sources were atmospheric deposition totaling 5.4 PBq and coastal discharge from a high-resolution coastal model totaling 4.5 PBq.

The tracer dispersed to a patch centered on the date line (180° longitude) for the surface on December 2012, with the tracer located mostly north of the Kuroshio Extension but also in the recirculation region south of the Kuroshio, and to depths mostly in the upper 400 m but reaching 700–1000 m. The maximum surface concentration initially declined rapidly, with the rate slowing down at about 5 months of the simulation, and resulting in maximum concentrations equal to 7 Bq m^{-3} on December 2012 and 5 Bq m^{-3} after 2 yr of simulation. The Kuroshio and the Kuroshio Extension, along with warm- and cold-core eddies, disperse and transport the tracer, while eddies, subduction along the Kuroshio front, and vertical mixing contribute to the migration of the tracer toward the subsurface. Our model suggested a possible pathway for transferring tracer across the front with the diving isopycnals corresponding to the intermediate water, taking surface tracer from the north of the front toward depths of 700–1000 m and locations south of the front, at longitudes where the surface Kuroshio front is well defined.

Compared to the observations of Buesseler et al. (2012) for June 2011, the model shows a reasonably correct tracer distribution but lower values by a factor of about 5. We can attribute part of these differences to the low surface concentrations used as the source for coastal discharge in our simulation. Incorporating simulated coastal discharge by the NOS-ROMS coastal simulation was a choice for us to achieve as much realism as possible under very time-sensitive circumstances. However, due to high vertical diffusion, the near-surface tracer coastal input was low. In addition, our direct discharge of 4.5 PBq is almost one-fourth of the total estimated by Rypina et al. (2013) to best fit the observations. With respect to the amount and distribution of the surface tracer, we notice that the observations contain the effects of continuous discharge that were not included in our simulation.

In comparison with the observations of Aoyama et al. (2013), the modeled results also give lower concentrations than observed. Reasons for this could be a horizontal distribution of atmospheric deposition that does not match the observations well enough. In addition, the tracer was diluted due to a deep modeled mixed layer depth, which is approximately twice that of the NAVOCEANO's hindcast. Our atmospheric deposition over land and ocean (10 PBq, of which 5.4 PBq were deposited over the ocean) is in total about one-third that of Stohl et al. (2012).

This operational model was decommissioned at the beginning of 2014, since the maximum surface ^{137}Cs concentrations were of the same magnitude as background values (2–5 $\mathrm{Bq\,m^{-3}}$), and the tracer patch had reached the eastern boundary. Future plans include correction of tracers concordant with incremental updates in the physical variables, with daily reinitialization of the model. Information provided to decision makers included gross guidance on areas that could be excluded from regions considered unsafe for human activity, for example Okinawa, Saipan, and Guam, in addition to Hawaii and Alaska. More timely observations would have been helpful for improving our estimations. We recommended that collaborators in MEXT in Japan take more surface observations from the region several hundred kilometers off of Fukushima during March–May 2011. In view of our simulated results, it would have been useful to obtain some profiles up to 700-m depth to better assess the redistribution of the surface waters into the ocean column.

Acknowledgments. Lyon Lanerolle kindly provided the NOS-ROMS solution for coastal discharge. Work described in this study was done using the computer and human resources at NOAA/NCEP. We thank two anonymous reviewers, and are especially grateful to one reviewer who provided substantial input for the improvement of this manuscript. We thank Dr. Hideyuki Kawamura from Japan Atomic Energy Agency for consultations.

APPENDIX A

Estimation of ^{137}Cs of Fukushima Origin through Synthetic Drifters

Immediately after the accident, but before the estimation of the radionuclide sources became available, we started estimating the tracer advection by following idealized synthetic drifters originated near FNPP (Tolman et al. 2013), using velocities from the now operational global ocean model at NCEP (RTOFS-Global hindcasts). This was done as an emergency procedure, with the aim of identifying regions where surface particles from the site of the accident migrate, as a function of time. The synthetic particles were kept at a depth of 3 m. Particles seeded in a 1/8° grid in a 2.2° × 1.4° region around FNPP (36°–37.4°N, 140.8°–143.0°E) dispersed 72 days afterward, staying mostly north of the Kuroshio and reaching a longitude about 168°E.

A low-resolution seeding grid (1/4° grid at 34°–44°N, 140°–162°E) was used together with the first estimates of atmospheric wet deposition from Nuclear Regulatory Commission model results (NRC-HYSPLIT-1) to obtain the activity over the ocean. The plume showed maximum activity of about 1000 $\mathrm{Bq\,m^{-3}}$ in the 32°–40°N, 140°–155°E region 37 days after the accident.

APPENDIX B

RTOFS-Global

RTOFS-Global uses HYCOM (Bleck 2002; Chassignet et al. 2003; Halliwell 2004) in the same configuration as the HYCOM GOFS hindcast at NAVOCEANO (Chassignet et al. 2009). RTOFS-Global has a 1/12° horizontal grid that is rectilinear south of 47°N (being equatorial Mercator except in the high southern latitudes) followed by an Arctic bipolar patch, and a vertical grid with 32 hybrid layers (isopycnal in the deep ocean, z levels in the ocean interior near the surface, and sigma coordinates near the coasts). The model's top layer is 3 m thick for dates earlier than 19 April 2011, while after that date, the top two layers have depths of 1 and 2 m. The potential density is referenced to the 20-MPa surface. The model's equation of state has thermobaric corrections, with potential density notated as σ_2^* (Sun et al. 1999; Chassignet et al. 2003). The model has a KPP mixed layer model (Large et al. 1994). Daily initializations are done at NAVOCEANO, using a multivariate optimal interpolation (MVOI) method through the Navy Coupled Ocean Data Assimilation (NCODA) system (Cummings 2005), assimilating available observations in incremental update cycles, including altimeter sea surface height anomaly; satellite, ship, and buoy sea surface temperatures; profiles from XBT, CTD, and Argo floats; and Special Sensor Microwave Imager (SSM/I) sea ice. For RTOFS-Global, each day, the hindcast cycle starts from an initial analysis corresponding to 2 days prior to the present produced at

NAVOCEANO. The model is advanced for 2 days in the past using hindcast forcing from NCEP's operational Global Data Assimilation System (GDAS) with data assimilation [http://www.ncdc.noaa.gov/model-data/global-data-assimilation-system-gdas; see also Kleist et al. (2009) and Saha et al. (2010) for the NCEP–NCAR reanalysis GDAS mentioned therein]. Then, six future forecast days are produced using NCEP's operational Global Forecast System (GFS) forcing [http://www.ncdc.noaa.gov/model-data/global-forcast-system-gfs; GFS forecasts are initialized with GDAS hindcast data; Yang et al. (2006)]. Daily radiation and temperature variations are included in the forcing for RTOFS-Global. A correction of air temperature is done to account for the difference between observed and GFS-GDAS-simulated ice coverage.

REFERENCES

Aoyama, M., D. Tsumune, and Y. Hamajima, 2012: Distribution of ^{137}Cs and ^{134}Cs in the North Pacific Ocean: Impacts of the TEPCO Fukushima–Daiichi NPP accident. *J. Radioanal. Nucl. Chem.*, **296**, 535–539, doi:10.1007/s10967-012-2033-2.

——, M. Uematsu, D. Tsumune, and Y. Hamajima, 2013: Surface pathway of radioactive plume of TEPCO Fukushima NPP1 released ^{134}Cs and ^{137}Cs. *Biogeosci. Discuss.*, **10**, 265–283, doi:10.5194/bgd-10-265-2013.

Barron, C. N., A. B. Kara, H. E. Hurlburt, C. Rowley, and L. F. Smedstad, 2004: Sea surface height predictions from the Global Navy Coastal Ocean Model during 1998–2001. *J. Atmos. Oceanic Technol.*, **21**, 1876–1893, doi:10.1175/JTECH-1680.1.

Behrens, E., F. U. Schwarzkopf, J. F. Lübbecke, and C. W. Böning, 2012: Model simulations on the long-term dispersal of ^{137}Cs released into the Pacific Ocean off Fukushima. *Environ. Res. Lett.*, **7**, 034004, doi:10.1088/1748-9326/7/3/034004.

Bleck, R., 2002: An oceanic general circulation model framed in hybrid isopycnic Cartesian coordinates. *Ocean Modell.*, **4**, 55–88, doi:10.1016/S1463-5003(01)00012-9.

Buesseler, K., M. Aoyama, and M. Fukasawa, 2011: Impacts of the Fukushima nuclear power plants on marine radioactivity. *Environ. Sci. Technol.*, **45**, 9931–9935, doi:10.1021/es202816c.

——, and Coauthors, 2012: Fukushima-derived radionuclides in the ocean and biota off Japan. *Proc. Natl. Acad. Sci. USA*, **109**, 5984–5988, doi:10.1073/pnas.1120794109.

Chassignet, E. P., L. T. Smith, G. R. Halliwell, and R. Bleck, 2003: North Atlantic simulations with the Hybrid Coordinate Ocean Model (HYCOM): Impact of the vertical coordinate choice, reference pressure, and thermobaricity. *J. Phys. Oceanogr.*, **33**, 2504–2526, doi:10.1175/1520-0485(2003)033<2504:NASWTH>2.0.CO;2.

——, and Coauthors, 2009: U.S. GODAE: Global Ocean Prediction with the HYbrid Coordinate Ocean Model (HYCOM). *Oceanography*, **22**, 64–75, doi:10.5670/oceanog.2009.39.

Chino, M., H. Nakayama, H. Nagai, H. Terada, G. Katata, and H. Yamazawa, 2011: Preliminary estimation of release amounts of ^{131}I and ^{137}Cs accidentally discharged from the Fukushima Daiichi nuclear power plant into the atmosphere. *J. Nucl. Sci. Technol.*, **48**, 1129–1134, doi:10.1080/18811248.2011.9711799.

Cummings, J. A., 2005: Operational multivariate ocean data assimilation. *Quart. J. Roy. Meteor. Soc.*, **131**, 3583–3604, doi:10.1256/qj.05.105.

Dietze, H., and I. Kriest, 2012: ^{137}Cs off Fukushima Dai-ichi, Japan—Model based estimates of dilution and fate. *Ocean Sci.*, **8**, 319–332, doi:10.5194/os-8-319-2012.

Draxler, R. R., and G. D. Hess, 1998: An overview of the HYSPLIT_4 modelling system for trajectories, dispersion, and deposition. *Aust. Meteor. Mag.*, **47**, 295–308.

——, and Coauthors, 2013: The World Meteorological Organization's evaluation of meteorological analysis for the radionuclide dispersion and deposition from the Fukushima Daiichi nuclear power plant accident. Report of the Third Meeting of WMO Task Team on Meteorological Analysis for Fukushima-Daiichi Nuclear Power Plant Accident, Annex III, World Meteorological Organization, 65 pp. [Available online at http://www.arl.noaa.gov/documents/reports/WMO_fnpp_final_AnnexIII_24Jan.pdf.]

——, and Coauthors, 2014: World Meteorological Organization's model simulations of the radionuclide dispersion and deposition from the Fukushima Daiichi nuclear power plant accident. *J. Environ. Radioact.*, doi:10.1016/j.jenvrad.2013.09.014, in press.

Estournel, C., and Coauthors, 2012: Assessment of the amount of cesium-137 released into the Pacific Ocean after the Fukushima accident and analysis of its dispersion in Japanese coastal waters. *J. Geophys. Res.*, **117**, C11014, doi:10.1029/2012JC007933.

Follows, M. J., and J. C. Marshall, 1994: Eddy driven exchange at ocean fronts. *Ocean Modell.*, **102**, 5–9.

Halliwell, G. R., 2004: Evaluation of vertical coordinate and vertical mixing algorithms in the HYbrid-Coordinate Ocean Model (HYCOM). *Ocean Modell.*, **7**, 285–322, doi:10.1016/j.ocemod.2003.10.002.

Haza, A. C., T. M. Özgökmen, A. Griffa, Z. D. Garraffo, and L. Peterbarg, 2012: Parameterization of particle transport at submesoscales in the Gulf Stream region using Lagrangian subgridscale models. *Ocean Modell.*, **42**, 31–49, doi:10.1016/j.ocemod.2011.11.005.

Honda, M. C., and Coauthors, 2012: Dispersion of artificial caesium-134 and -137 in the western North Pacific one month after the Fukushima accident. *Geochem. J.*, **46**, e1–e9, doi:10.2343/geochemj.1.0152.

Kamenik, J., H. Dulalova, K. Buesseler, S. Pike, and K. Šťatná, 2013: Cesium-134 and 137 activities in the central North Pacific Ocean after the Fukushima Dai-ichi nuclear power plant accident. *Biogeosciences*, **10**, 6045–6052, doi:10.5194/bg-10-6045-2013.

Kanda, J., 2013: Continuing ^{137}Cs release to the sea from the Fukushima Dai-ichi nuclear power plant through 2012. *Biogeosciences*, **10**, 6107–6113, doi:10.5194/bg-10-6107-2013.

Kawabe, M., 1995: Variations in current path, velocity, and volume transport of the Kuroshio in relation with the large meander. *J. Phys. Oceanogr.*, **25**, 3103–3117, doi:10.1175/1520-0485(1995)025<3103:VOCPVA>2.0.CO;2.

Kawai, H., 1972: Hydrography of the Kuroshio Extension. *Kuroshio—Its Physical Aspects,* H. Stommel and K. Yoshida, Eds., University of Tokyo Press, 235–352.

Kawamura, H., T. Kobayashi, A. Furuno, T. In, Y. Ishikawa, T. Nakayama, S. Shima, and T. Awaji, 2011: Preliminary numerical experiments on oceanic dispersion of ^{131}I and ^{137}Cs discharged into the ocean because of Fukushima Daiichi nuclear power plant disaster. *J. Nucl. Sci. Technol.*, **48**, 1349–1356, doi:10.1080/18811248.2011.9711826.

Kleist, D. T., D. F. Parrish, J. C. Derber, R. Treadon, W.-S. Wu, and S. Lord, 2009: Introduction of the GSI into the NCEP Global Data Assimilation System. *Wea. Forecasting*, **24**, 1691–1705, doi:10.1175/2009WAF2222201.1.

Large, W. G., J. C. McWilliams, and S. C. Doney, 1994: Oceanic vertical mixing: A review and a model with a nonlocal boundary layer parameterization. *Rev. Geophys.*, **32**, 363–403, doi:10.1029/94RG01872.

Lumpkin, R., and Z. Garraffo, 2005: Evaluating the decomposition of tropical Atlantic drifter observations. *J. Atmos. Oceanic Technol.*, **22**, 1403–1415, doi:10.1175/JTECH1793.1.

Marshall, D., 1997: Subduction of water masses in an eddying ocean. *J. Mar. Res.*, **55**, 201–222, doi:10.1357/0022240973224373.

Masumoto, Y., and Coauthors, 2012: Oceanic dispersion simulations of ^{137}Cs released from the Fukushima Daiichi Nuclear Power Plant. *Elements*, **8**, 207–212, doi:10.2113/gselements.8.3.207.

Mensa, J. A., Z. Garraffo, A. Griffa, T. M. Özgökmen, A. Haza, and M. Veneziani, 2013: Seasonality of the submesoscale dynamics in the Gulf Stream region. *Ocean Dyn.*, **63**, 923–941, doi:10.1007/s10236-013-0633-1.

Mizuno, K., and W. B. White, 1983: Annual and interannual variability in the Kuroshio current system. *J. Phys. Oceanogr.*, **13**, 1847–1867, doi:10.1175/1520-0485(1983)013<1847:AAIVIT>2.0.CO;2.

Morino, Y., T. Ohara, and M. Nishizawa, 2011: Atmospheric behavior, deposition, and budget of radioactive materials from the Fukushima Daiichi nuclear power plant in March 2011. *Geophys. Res. Lett.*, **38**, doi:10.1029/2011GL048689.

Niiler, P. P., N. A. Maximenko, G. G. Panteleev, T. Yamagata, and D. B. Olson, 2003: Near-surface dynamical structure of the Kuroshio Extension. *J. Geophys. Res.*, **108**, 3193, doi:10.1029/2002JC001461.

Oka, E., and T. Suga, 2005: Differential formation and circulation of North Pacific central mode water. *J. Phys. Oceanogr.*, **35**, 1997–2011, doi:10.1175/JPO2811.1.

——, and B. Qiu, 2012: Progress of North Pacific mode water research in the past decade. *J. Oceanogr.*, **68**, 5–20, doi:10.1007/s10872-011-0032-5.

Pollard, R. T., and L. A. Regier, 1992: Vorticity and vertical circulation at an ocean front. *J. Phys. Oceanogr.*, **22**, 609–625, doi:10.1175/1520-0485(1992)022<0609:VAVCAA>2.0.CO;2.

Qiu, B., 2001: Kuroshio and Oyashio Currents. *Encyclopedia of Ocean Sciences,* J. Steele, Ed., Academic Press, 1413–1425.

Rossi, V., E. V. Sebille, A. S. Gupta, V. Garon, and M. England, 2013: Multi-decadal projections of surface and interior pathways of the Fukushima cesium-137 radioactive plume. *Deep-Sea Res. I*, **80**, 37–46, doi:10.1016/j.dsr.2013.05.015.

Rypina, I. I., S. R. Jayne, S. Yoshida, A. M. Macdonald, E. Douglass, and K. Buesseler, 2013: Short-term dispersal of Fukushima-derived radionuclides off Japan: Modeling efforts and model–data intercomparison. *Biogeosci. Discuss.*, **10**, 1517–1550, doi:10.5194/bgd-10-1517-2013.

Saha, S., and Coauthors, 2010: The NCEP Climate Forecast System Reanalysis. *Bull. Amer. Meteor. Soc.*, **91**, 1015–1057, doi:10.1175/2010BAMS3001.1.

Stohl, A., and Coauthors, 2012: Xenon-133 and caesium-137 releases into the atmosphere from the Fukushima Dai-ichi nuclear power plant: Determination of the source term, atmospheric dispersion, and deposition. *Atmos. Chem. Phys.*, **12**, 2313–2343, doi:10.5194/acpd-11-28319-2011.

Suga, T., K. Motoki, Y. Aoki, and A. Macdonald, 2004: The North Pacific climatology of winter mixed layer and mode waters. *J. Phys. Oceanogr.*, **34**, 3–22, doi:10.1175/1520-0485(2004)034<0003:TNPCOW>2.0.CO;2.

Sun, S., R. Bleck, C. Rooth, J. Dukowicz, E. Chassignet, and P. Killworth, 1999: Inclusion of thermobaricity in isopycnic-coordinate ocean models. *J. Phys. Oceanogr.*, **29**, 2719–2729, doi:10.1175/1520-0485(1999)029<2719:IOTIIC>2.0.CO;2.

Talley, L. D., 1993: Distribution and formation of North Pacific Intermediate Water. *J. Phys. Oceanogr.*, **23**, 517–537, doi:10.1175/1520-0485(1993)023<0517:DAFONP>2.0.CO;2.

Tolman, H. L., Z. Garraffo, A. Mehra, I. Rivin, and T. Spindler, 2013: Ocean plume and tracer modeling for the Fukushima Dai'ichi event: Particle tracking. MMAB/EMC/NOAA Tech. Note 309, 111 pp. [Available online at http://polar.ncep.noaa.gov/mmab/papers/tn309/MMAB_309.pdf.]

Tsumune, D., T. Tsubono, M. Aoyama, and K. Hirose, 2012: Distribution of oceanic ^{137}Cs from the Fukushima Dai-ichi Nuclear Power Plant simulated numerically by a regional ocean model. *J. Environ. Radioact.*, **111**, 100–108, doi:10.1016/j.jenvrad.2011.10.007.

——, ——, ——, M. Uematsu, K. Musumi, Y. Maeda, Y. Yoshida, and H. Hayami, 2013: One-year, regional-scale simulation of ^{137}Cs radioactivity in the ocean following the Fukushima Dai-ichi Nuclear Power Plant accident. *Biogeosciences*, **10**, 5601–5617, doi:10.5194/bg-10-5601-2013.

Yang, F., H.-L. Pan, S. K. Krueger, S. Moorthi, and S. J. Lord, 2006: Evaluation of the NCEP Global Forecast System at the ARM SGP site. *Mon. Wea. Rev.*, **134**, 3668–3690, doi:10.1175/MWR3264.1.

Yasuda, I., 2003: Hydrographic structure and variability in the Kuroshio–Oyashio transition area. *J. Oceanogr.*, **59**, 389–402, doi:10.1023/A:1025580313836.

——, K. Okuda, and Y. Shimizu, 1996: Distribution and modification of North Pacific Intermediate Water in the Kuroshio–Oyashio interfrontal zone. *J. Phys. Oceanogr.*, **26**, 448–465, doi:10.1175/1520-0485(1996)026<0448:DAMONP>2.0.CO;2.

You, Y., 2003: The pathway and circulation of North Pacific Intermediate Water. *Geophys. Res. Lett.*, **30,** 2291, doi:10.1029/2003GL018561.

——, N. Suginohara, M. Fukasawa, H. Yoritaka, K. Mizuno, Y. Kashino, and D. Hartoyo, 2003: Transport of North Pacific Intermediate Water across Japanese WOCE sections. *J. Geophys. Res.*, **108**, 3196, doi:10.1029/2002JC001662.